

Multi-criteria Comparison among Several Mitigation Strategies for Dangerous Near Earth Objects

*J.P. Sanchez**, *C. Colombo†*, *M. Vasile‡* and *G. Radice§*

University of Glasgow, Glasgow, G12 8QQ, United Kingdom

In this paper a comparative assessment of the effectiveness of different deviation methods for Near Earth Objects is presented. Specifically, solar collector, nuclear interceptor, kinetic impactor, low-thrust propulsion, mass driver and gravity tug are modeled and compared. For each method, a mathematical model is developed in order to compute the achievable deviation. A multi-criteria optimization method is then used to construct the set of Pareto optimal solutions, minimizing the mass of the spacecraft at departure from the Earth and the warning time, i.e., the time from launch to the foreseen impact of the asteroid with the Earth, while at the same time maximizing the deviation. A dominance criterion is defined and used to compare all the Pareto sets for all the various mitigation strategies. Finally a Technology Readiness Level factor is associated to each strategy in order to estimate the required technological development.

Nomenclature

A_m	=	cross section area of the mirror, m^2
A_s	=	area of the illuminated spot, m^2
a	=	semi-major axis of an orbit, km
b	=	semi-minor axis of an orbit, km
c	=	heat capacity, J/kg/K
d	=	hovering distance, m
E_A	=	received energy per unit area, J/m^2

** Ph.D. Candidate, Department of Aerospace Engineering, James Watt (South Building), psanchez@eng.gla.ac.uk.

† Ph.D. Candidate, Department of Aerospace Engineering, James Watt (South Building), ccolombo@eng.gla.ac.uk.

‡ Lecturer Ph.D., Department of Aerospace Engineering, James Watt (South Building), mvasile@eng.gla.ac.uk, AIAA Member.

§ Senior Lecturer Ph.D., Department of Aerospace Engineering, James Watt (South Building), gradice@eng.gla.ac.uk, AIAA Member.

E_t	=	total energy released by the nuclear interceptor, J
E_v	=	energy of sublimation, J/g
e	=	eccentricity of an orbit
$erfc(f(x))$	=	complementary error function of $f(x)$
F_g	=	gravity attraction between the spacecraft and the asteroid, N
F_{hover}	=	effective vertical thrust, N
G	=	universal gravitational constant, $6.67259 \times 10^{-11} \text{ m}^3/\text{kg/s}^2$
g_0	=	standard free fall constant, 9.81 m/s^2
H	=	altitude of detonation of the nuclear interceptor, m
h	=	distance from the nuclear explosion to a specific point on the surface of the asteroid, m
I_{sp}	=	specific impulse of a propulsion system, s
i	=	inclination of an orbit, deg
k	=	Boltzman constant, $1.380658 \times 10^{-23} \text{ J/K}$
M	=	mean anomaly of an orbit, deg
M_a	=	mass of the asteroid, kg
M_m	=	molecular mass, kg
m_A	=	mass per unit area, kg/m^2
m_d	=	dry mass of the spacecraft, kg
m_{debris}	=	mass of the nuclear interceptor's debris that impacts the asteroid, kg
m_i	=	mass of the spacecraft at the Near Earth Object arrival, kg
m_{launch}	=	mass expelled per shot by the Mass driver method, kg
m_{power}	=	mass of the power subsystem, kg
m_{wh}	=	mass of the nuclear warhead, kg
m_0	=	mass launched into space, kg
n	=	angular velocity of an orbit, s^{-1}
p_A	=	linear momentum per unit area, kg/s/m
P_K	=	kinetic power provided by the mass driver, W
P_{in}	=	radiation power density over the illuminated surface of the asteroid, W/m^2
p	=	semilatus rectum of an orbit, km
Q_{cond}	=	heat flux loss by conduction, W/m^2

Q_{rad}	=	heat flux loss by radiation, W/m ²
R_a	=	mean radius of the Near Earth Object, m
r_{fi}	=	distance from spacecraft to the Sun, km
S_{flux}	=	solar flux at 1 AU, 1367 W/m ²
S_{sc}	=	scattering factor
T	=	temperature, K
T_n	=	thrust, N
t	=	time, s or d
t_0	=	time at which a low thrust deviation maneuver begins or an impulsive maneuver occurs,
s or d		
t_f	=	time at which the deviation maneuver is completed, s or d
t_{MOID}	=	time at the Minimum Orbit Interception Distance point, s or d
t_{push}	=	duration of the pushing action, s
\bar{V}	=	average velocity of evaporated particles, m/s
v_{debris}	=	velocity of the debris from the nuclear Interceptor, m/s
V_{rot}	=	rotational velocity of the asteroid equatorial surface, m/s
v_e	=	excess velocity of the expelled or sublimated material, m/s
v	=	orbital velocity, km/s
YTW	=	yield-to-weight ratio of the nuclear device, kTons/ kg
z	=	asteroid depth, m
Z_{max}	=	maximum radiation depth, m
β	=	momentum enhancement factor
$\Delta \mathbf{r}$	=	vector distance at the Minimum Orbit Interception Distance, km
$\Delta \mathbf{v}_{S/C}$	=	relative velocity of the spacecraft with respect to the asteroid, m/s or km/s
$\Delta t_{shooting}$	=	time available to shoot the dug material, s
$\delta \mathbf{r}$	=	deviation vector in the Hill coordinate frame, km
$\delta \mathbf{v}$	=	impulsive change of velocity vector, m/s or km/s
δv	=	scalar increment of velocity, m/s or km/s
ε	=	elevation angle, deg

ε_{bb}	=	black body emissivity
η	=	spacecraft-centered nadir angle, deg
η_{eff}	=	efficiency of the mirror assembly
θ	=	true anomaly of an orbit , deg
θ^*	=	argument of latitude of an orbit, deg
k	=	thermal conductivity, W/m/K
λ	=	asteroid central angle, deg
μ_o	=	opacity of a material to a certain radiation, m ² /kg
ν	=	angle between the orbital velocity and the \hat{x} axis of the ecliptic inertial reference frame,
deg		
ξ	=	specific thrust, N/W
ϖ	=	complementary latitude angle, deg
ρ_a	=	mean density of the asteroid, kg/m ³
σ	=	Stefann-Boltzmann constant, 5.67051×10^{-8} W/m ² /K ⁴
τ	=	mass-to-power ratio, kg/W
ϕ	=	exhaust cone half-angle, deg
Ω	=	argument of the ascending node of an orbit, deg
ω	=	argument of the perigee of an orbit, deg

Subscripts

$()_t$	=	vector component tangent to the orbit
$()_n$	=	vector component normal to the orbit in the orbit plane
$()_h$	=	vector component normal to the orbit plane

I. Introduction

Over the last few years, the possible scenario of an asteroid threatening to impact the Earth has stimulated an intense debate among the scientific community about possible deviation methods. Small celestial bodies like Near Earth Objects (NEOs) have become a common subject of study because of their importance in uncovering the mysteries of the formation, evolution and composition of the solar system. Among all asteroids, NEOs have stepped into prominence because of two important aspects: they are

among the easiest celestial bodies to reach from Earth, in some cases they can be reached with less demanding trajectories than a simple Earth-Moon trajectory and, even more meaningful, they may represent a threat to our planet.

On average, every 26-30 million years a 10-km-sized asteroid strikes the Earth, while every several hundred years there is a Tunguska class (100 m in diameter) asteroid impact¹. Each of these impacts permanently alters the characteristics of our planet to varying degrees. These events, and the risks they pose to our fragile ecosystem, have made the space community turn their attention to the NEO issue².

Evidence of this new-found interest is the prolific and successful asteroid exploration program of the last decade, with many completed missions such as NEAR, Deep Space 1, Deep Impact or Stardust, ongoing missions like Rosetta, Hayabusa and Dawn and future missions such as Don Quijote, which will not only study the target asteroid but also test the capability to deflect its course with a high velocity impact.

In order to predict the effects of a deflection strategy, some studies have addressed the asteroid deviation problem either with an analytical approach^{3;4} or by means of a numerical procedure based on a n -body model⁵. Previous deflection formulas considered only a change in the orbital period due to an action applied along the direction of the motion of the asteroid. A more general approach was proposed by Conway⁶ to determine the near-optimal direction in which the impulse should be applied in order to maximize the consequent deviation. A similar approach was taken by Park and Ross⁷, who also took into consideration the gravitational effects of the Earth⁸, obtaining a more accurate estimation of the optimal impulse.

A few authors have performed a partial comparative assessment of the numerous proposed mitigation strategies. Some of these emphasize a classification system based on NEO/spacecraft coupling⁹, other systems are based on technology readiness and a third category on time to impact and/or intervention on the asteroid. On the other hand since the day the first mitigation technique¹⁰ was proposed, many approaches have been put forward by several scientists and a comprehensive quantitative comparison is still lacking.

All these different techniques can be grouped into several families depending on the type of asteroid-spacecraft interaction: techniques producing an impulsive change in the linear momentum of the asteroid, such as kinetic impactors and nuclear interceptors¹¹⁻¹³; techniques actively producing a controlled continuous low-thrust, such as attached propulsion devices⁴ (e.g., electric/chemical engines, solar sails) or

gravitational tugs¹⁴; techniques producing a passive low-thrust by an induced change of the thermo-optical properties of the asteroid surface¹⁵, such as enhanced Yarkovsky effect or enhanced emissivity through white paint; techniques producing a controlled thrust by the ablation of the asteroid surface¹⁶ (e.g., through laser beams or solar collectors); or techniques producing a multi-impulsive change of the asteroid linear momentum by the ejection of surface material, such as the mass driver¹⁷.

This paper presents a comparison of deflection methods according to a set of different criteria. A collection of NEOs, differing in physical characteristics (i.e. size, mass and spin properties) and orbital parameters, was selected for this analysis. A group of different mitigation strategies taken from the families listed above, was then applied to these asteroids and evaluated in terms of four figures of merit: achieved miss distance at the Earth, warning time, total mass into orbit and technology readiness level, i.e. the estimated time to develop the technology required to implement a given mitigation strategy.

The first three criteria (miss distance, warning time and mass into orbit) express quantitatively how easy deflecting an asteroid with a given method is and whether we can implement a given deviation strategy with present launch capabilities. The warning time, in particular, besides giving quantitative information on the time to react (how far in advance we need to know that an impact is going to occur), it gives an indication on the time available to repair a failed deflection operation.

Finally the paper presents a multi-criteria optimization which provides a preliminary and relative measure of the effectiveness of one deviation over another according to the selected criteria.

II. Deviation Formulas and Maximum Deviation Problem

Given the Minimum Orbit Interception Distance (MOID) from the Earth for a generic Near Earth Object, the objective is to maximize the MOID by applying a deviation action. The effect on the asteroid of all the deviation strategies in this paper, was modeled either as an impulsive $\Delta \mathbf{v}$ at the interception time t_0 or as a continuous acceleration over the interval $[t_0 \ t_f]$ where t_f is the time in which the deviation maneuver is completed. The achieved miss distance is computed by means of proximal motion equations¹⁸ expressed as a function of the variation of the orbital elements. The variation of the orbital elements is computed with Gauss' planetary equations¹⁹.

The deviation maneuver acts as a perturbation on the orbit of the asteroid and the new orbit can be considered proximal to the unperturbed one. If θ_{MOID} is the true anomaly of the NEO at the MOID point along the unperturbed orbit and $\theta_{MOID}^* = \theta_{MOID} + \omega$ the corresponding argument of latitude, we can write

the variation of the position of the NEO, after deviation, with respect to its unperturbed position by using the proximal motion equations:

$$\begin{aligned}
\delta s_r &\approx \frac{r}{a} \delta a + \frac{ae \sin \theta_{MOID}}{\eta} \delta M - a \cos \theta_{MOID} \delta e \\
\delta s_\theta &\approx \frac{r}{\eta^3} (1 + e \cos \theta_{MOID})^2 \delta M + r \delta \omega + \frac{r \sin \theta_{MOID}}{\eta^2} (2 + e \cos \theta_{MOID}) \delta e + r \cos i \delta \Omega \\
\delta s_h &\approx r (\sin \theta_{MOID}^* \delta i - \cos \theta_{MOID}^* \sin i \delta \Omega)
\end{aligned} \tag{1}$$

where δs_r , δs_θ and δs_h are the displacements in the radial, transversal and perpendicular to the orbit plane directions respectively, so that $\delta \mathbf{r} = [\delta s_r \quad \delta s_\theta \quad \delta s_h]^T$, and $\eta = \sqrt{1 - e^2}$.

In the case of an impulsive action on the asteroid, the variation of the orbital parameters a , e , i , Ω and ω between the unperturbed and the proximal orbit are computed through Gauss' planetary equations written for an instantaneous change in the NEO velocity vector $\delta \mathbf{v} = [\delta v_t \quad \delta v_n \quad \delta v_h]^T$, where the components of this vector are expressed in the tangential, normal and perpendicular to the orbit plane directions, at $\theta = \theta_0$:

$$\begin{aligned}
\delta a &= \frac{2a^2 v}{\mu} \delta v_t \\
\delta e &= \frac{1}{v} \left[2(e + \cos \theta_0) \delta v_t - \frac{r}{a} \sin \theta_0 \delta v_n \right] \\
\delta i &= \frac{r \cos \theta_0^*}{h} \delta v_h \\
\delta \Omega &= \frac{r \sin \theta_0^*}{h \sin i} \delta v_h \\
\delta \omega &= \frac{1}{ev} \left[2 \sin \theta_0 \delta v_t + \left(2e + \frac{r}{a} \cos \theta_0 \right) \delta v_n \right] - \frac{r \sin \theta_0^* \cos i}{h \sin i} \delta v_h
\end{aligned} \tag{2}$$

and with the total variation in the mean anomaly:

$$\delta M = -\frac{b}{eav} \left[2 \left(1 + \frac{e^2 r}{p} \right) \sin \theta_0 \delta v_t + \frac{r}{a} \cos \theta_0 \delta v_n \right] + \delta n (t_{MOID} - t_0) \tag{3}$$

Eq. (3) takes into account the instantaneous change of the orbit geometry at time t_0 and the change in the mean anomaly at the time of the MOID due to a change in the semi-major axis, given by $\delta n(t_{MOID} - t_0)$, where t_{MOID} is the time at the MOID point along the orbit of the NEO and

$$\delta n = \sqrt{\frac{\mu}{(a + \delta a)^3}} - \sqrt{\frac{\mu}{a^3}}.$$

When a continuous deviation action is selected instead, the total variation of the orbital parameters is computed by numerically integrating Gauss' variational equations over the interval $[t_0 \ t_f]$, applying the acceleration produced by the deviation strategy. In this case the variation of the mean anomaly is computed in a similar fashion to Eq. (3):

$$\delta M = (n_f - n)t_{MOD} + nt_0 - n_f t_f + \Delta M \quad (4)$$

where n is the nominal angular velocity, n_f is the mean motion at time t_f and ΔM is calculated through the numerical integration of Gauss' equations.

III. Asteroid Deflection Strategies

In this paper we analyze and compare six deflection strategies: solar collector, nuclear interceptor, kinetic impactor, low-thrust propulsion, mass driver and gravity tug. In order to study the effectiveness of each deviation strategy, a set of mathematical models was developed to compute the variation of the linear momentum of a NEO, due to each one of the deviating actions. The deviating action produced by kinetic impactor and nuclear interceptors was modeled as an impulsive variation of the NEO's velocity, while the deviating actions provided by low-thrust propulsion, gravity tug and solar collector were modeled as a continuous variation of the asteroid linear momentum. The effect of mass drivers, instead, was modeled as a sequence of impulses, thus as a discrete variation of the linear momentum of the asteroid.

It is assumed that, for kinetic impactors and nuclear interceptors the direction of the deviating impulse depends only on the transfer trajectory from the Earth to the asteroid and is aligned with the relative velocity vector between the spacecraft and the asteroid at the end of the transfer. For all the other strategies, instead, the direction of the deviating action is independent of the transfer, thus we chose the closest direction to the theoretical optimal one²⁰.

The remainder of this section contains a description of the mathematical models for the six above-mentioned deviations methods. Some of the models are taken from the existing literature and adapted to the present analysis, while others represent a new development with respect to what already is in the literature.

A. Nuclear Interceptor

Nuclear devices are able to carry the highest energy density among all the deviation methods currently available. Not surprisingly the first deviation strategy ever proposed¹⁰ already suggested the use of nuclear bombs to change the collision course of an asteroid. On the other hand, it is worthwhile to remark that this technology could represent a significant risk. As pointed out by Carl Sagan in the *Pale Blue Dot*²¹, all mitigation technologies can be a double-edge sword if misused, but for obvious reasons delivering nuclear warheads in space could represent a higher menace than other deflection methods. This fearsome risk, intrinsic to this technology, would most probably arise political and security issues, which would certainly make the development of a deflection strategies based in nuclear weapons not only a technological problem. However, the work described here has not considered those additional issues.

The model used in this study is based on a stand-off configuration over a spherical asteroid. This type of configuration requires detonating the nuclear charge at distance H from the asteroid surface (Fig. 1). The method is less sensitive to possible uncertainties in the asteroid composition and surface morphology²², unlike other nuclear-based configurations, such as buried and surface explosions.

The energy released during a nuclear explosion is carried mainly by X-rays, neutrons, gamma radiation and debris and its distribution depends mostly on the type of nuclear reaction.

Table 1 shows the distribution of energy used in this work, which is taken from Hammerling²² and based on the information in Glasstone²³. As can be read in the table, an important part of the total energy is carried, in the form of kinetic energy, by the debris resulting from the explosion. Although its momentum coupling, or efficiency in producing linear momentum change, is much smaller than the one of the radioactive processes (see Fig. 3), still its effect cannot be neglected. In the following, a model for the computation of the change in the velocity of the asteroid due to debris and radiation is presented.

Table 1: Energy Distribution

Source	X-ray	Neutrons	Gamma-rays	Debris	Others
Fission	70%	1%	2%	20%	7%
Fusion	55%	20%	1%	20%	4%

1. Debris

After the detonation of the nuclear device, part of the debris, from the spacecraft structure and components, will impact the surface of the asteroid. Assuming that the explosion produces a spherical shock wave and the debris is homogeneously distributed on the surface of this shock wave, the total

amount of debris impacting the asteroid m_{debris} is given by the dry mass of the spacecraft m_d multiplied by the ratio S between the total area of the shock wave and the portion of it that intersects the asteroid:

$$m_{debris} = Sm_d \quad (5)$$

where S is defined as:

$$S = \frac{1}{2} - \frac{\sqrt{H}}{2} \frac{\sqrt{H+2R_a}}{R_a+H} \quad (6)$$

Here and in the following the dry mass m_d is the mass of the spacecraft without the propellant to perform the transfer from the Earth to the asteroid. The impacting velocity of the debris v_{debris} is then given by:

$$v_{debris} = \sqrt{\frac{2f_{debris}E_t}{m_d}} \quad (7)$$

where E_t is the total yield release by the nuclear interceptor and f_{debris} is the fraction of delivered energy in kinetic form (see Table 1). The final increment in the asteroid velocity δv_{debris} is calculated by using the conservation of linear momentum:

$$\delta v_{debris} \approx \beta S_{Sc} \frac{m_{debris} v_{debris}}{M_a} \quad (8)$$

where S_{Sc} is a scattering factor, β is the momentum enhancement factor¹¹ and M_a is the mass of the asteroid.

2. Radiations

Following the Beer-Lambert law of absorption, the radiant energy absorbed per unit area by a layer of material of thickness dz and mass per unit area $dm_A = \rho_a dz$ is:

$$dE_A = -\mu_0 E_A dm_A \quad (9)$$

where μ_0 is the opacity of the material and E_A is the received energy per unit area and ρ_a is the mean density of the asteroid, The opacity μ_0 , or linear mass-absorption coefficient, describes how the energy is absorbed as it passes through the asteroid and its value depends on the radiation type, the associated energy and the material considered. In this study, we assumed that the asteroid's surface was mainly made of forsterite and that the energy of the impacting radiation was in the range of 10 keV for X-ray, 2 MeV for gamma-ray and 14 MeV for neutron radiation²²; with these hypotheses the opacity for different radiations has the values in Table 2.

Table 2: Opacity or linear mass-absorption coefficient for an asteroid made of forsterite

Opacity	X-ray	Neutron	Gamma-ray
μ_0	1.5 m ² /kg	0.0044 m ² /kg	0.005 m ² /kg

Thus the energy per unit area varies with the depth z is:

$$\frac{dE_A}{dz} = -\mu_0 \rho_a E_A \quad (10)$$

which, when integrated over z , gives the amount of energy per unit area remaining at a given depth:

$$E_A(z) = E_A(0) e^{-\rho_a \mu_0 z} \quad (11)$$

where $E_A(0)$ is the energy on the external surface, which depends on the distance from the explosion. The absorbed energy at a specific depth z per unit area and unit mass, $\mu_0 E_A(z)$, induces the sublimation of material. A portion E_v of the energy goes into the sublimation process (sublimation enthalpy), while the remaining energy is converted into kinetic energy and accelerates the sublimated material up to a velocity v_e given by:

$$v_e = \sqrt{2(\mu_0 E_A(z) - E_v)} \quad (12)$$

If we consider forsterite (i.e. Mg₂SiO₄) as the main component of the asteroids, then the sublimation enthalpy is $E_v = 5.03$ kJ/g (Wang²⁴). This assumption is likely to represent a worse case scenario since the surface of the asteroid might have more volatile materials, and the regolith may even help to increase the thrust/energy efficiency. The variation of the linear momentum per unit area dp_A gained by the asteroid due to the evaporated mass is:

$$dp_A = \rho_a v_e dz \quad (13)$$

which integrated from the surface of the asteroid to the maximum depth at which the evaporation takes place, Z_{\max} , gives the total linear momentum per unit area:

$$P_A = \int_0^{Z_{\max}} dp_A dz \quad (14)$$

The maximum depth Z_{\max} can be computed as follows:

$$Z_{\max} = \frac{1}{\rho_a \mu_0} \ln \left(\frac{\mu_0 E_A(0)}{E_v} \right) \quad (15)$$

Taking into account the elevation angle ε of the incoming radiation (see Fig. 1), the linear momentum per unit area p_A becomes:

$$P_A = \int_0^{Z_{\max} \sin \varepsilon} \rho_a \sqrt{2 \left(\mu_o E_A(0) e^{-\rho_a \mu_o \frac{z}{\sin \varepsilon}} - E_v \right)} dz \quad (16)$$

The integration of Eq. (13), but without the velocity v_e , gives the mass ablated from the asteroid surface:

$$m_{\text{ablated}} = \int_0^{Z_{\max} \sin \varepsilon} \rho_a dz \quad (17)$$

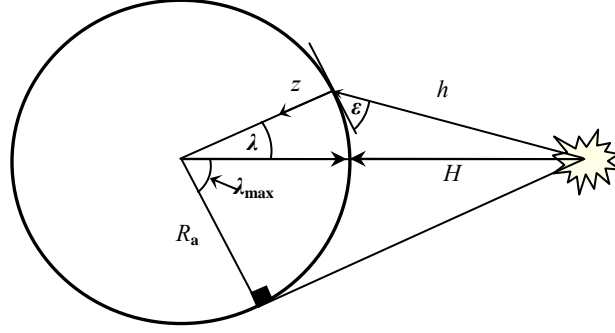


Fig. 1 Geometric diagram of the spacecraft detonation and asteroid.

Eq. (16) can now be integrated over the entire radiated surface. Using the equation of the surface of a spherical cap (see Fig. 2):

$$S_{\text{cap}} = 2\pi R_a^2 (1 - \cos \lambda) \quad (18)$$

we obtain an integration only dependant on the asteroid central angle λ , which leads to the following double integration:

$$P = \sqrt{8\pi} R_a^2 \rho_a \int_0^{\lambda_{\max}} \left(\int_0^{Z_{\max} \sin \varepsilon(\lambda)} \left(\mu_o \frac{f_{\text{radiation}} E_t}{4\pi [h(\lambda)]^2} e^{-\frac{\rho_a \mu_o z}{\sin \varepsilon(\lambda)}} - E_v \right)^{1/2} dz \right) \sin \lambda d\lambda \quad (19)$$

where E_t is the total energy released by the explosion, $f_{\text{radiation}}$ is the fraction of energy corresponding to each one of the three radiations in Table 1, and h is the distance from the explosion to the surface of the asteroid. The distance h is expressed as a function of the central angle $\lambda \in [0 \ \lambda_{\max}]$ (see Fig. 1), where λ_{\max} corresponds to the distance to the horizon of the asteroid as seen from the spacecraft. Finally, the $\delta v_{\text{radiation}}$ experienced by the asteroid is calculated by integrating Eq. (19) and dividing it by the total mass of the asteroid.

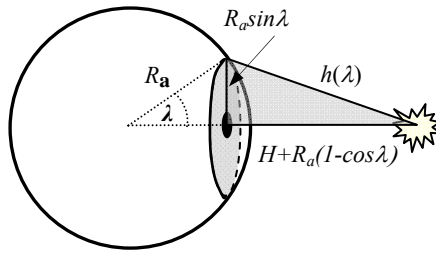


Fig. 2 Integration over the spherical cap.

Fig. 3 shows the total δv given by the combination of all four components (i.e. X-ray, neutron radiation, gamma radiation and debris) as well as the individual contribution of each as a function of H . In this example, the spacecraft was carrying a nuclear fusion device with a mass of 600 kg in the proximity of the asteroid Apophis. Fig. 3 shows that the neutron radiation gives the highest contribution to the total δv ; note that the same conclusion is valid even for a nuclear fission device. The optimal stand-off distance is $H = 0.15R_a$, where the maximum total increment of velocity occurs.

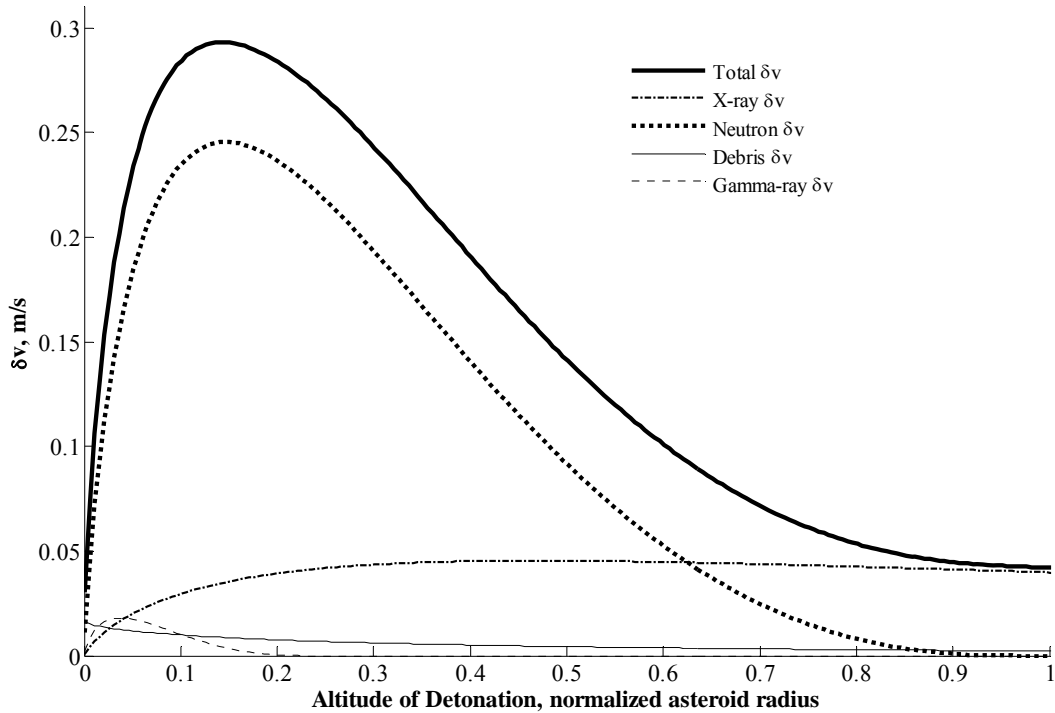


Fig. 3 Change in velocity of asteroid Apophis achieved with a Nuclear Interceptor carrying a fusion device of 600 kg, as a function of altitude of detonation H . The distance is normalized using the asteroid average radius.

The ablated mass $m_{ablated}$ and the average velocity of the sublimated material coming from each one of the types of radiation are plotted in Fig. 4. It can be observed that X-rays produce very high excess velocities but ablate a very thin layer of material from the surface of the asteroid. On the other hand,

neutron radiation produces more evaporation, since this radiation penetrates deeper into the asteroid and this is a more efficient way of providing impulse to the asteroid. The total impulsive action is therefore the sum of all the individual contributions:

$$\delta v = \delta v_{\text{gamma}} + \delta v_{\text{X-rays}} + \delta v_{\text{debris}} + \delta v_{\text{neutrons}} \quad (20)$$

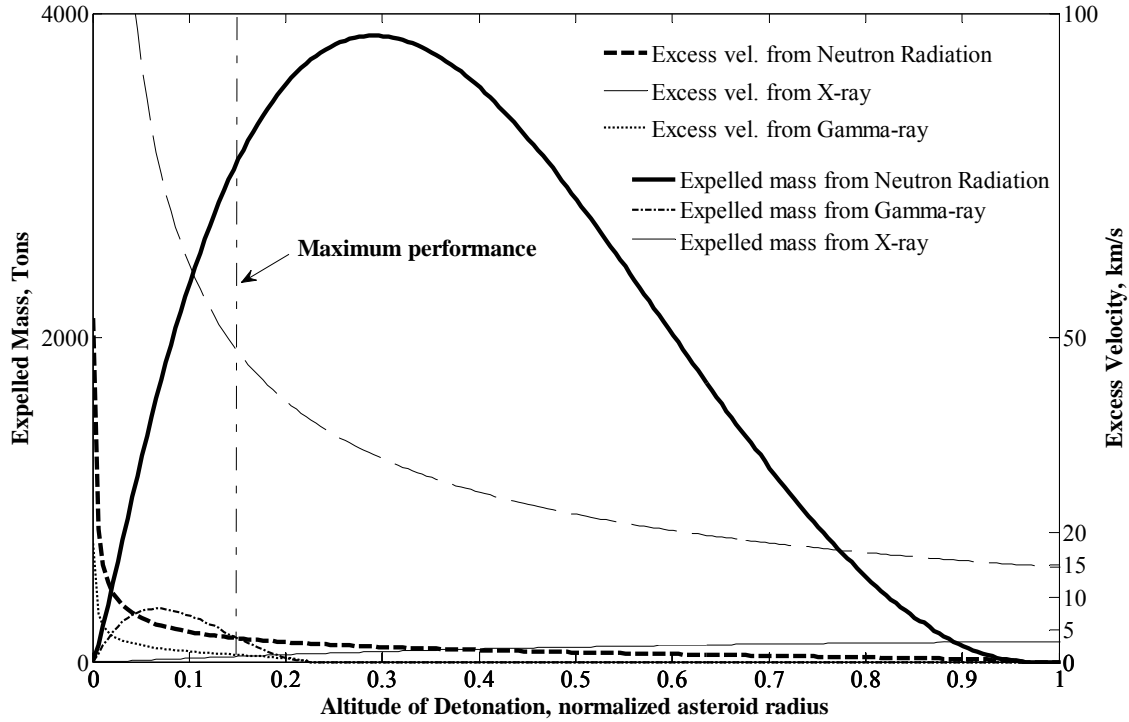


Fig. 4 Radiation analysis. *Y* axis on the left shows the mass evaporated by the three main radiation components of the nuclear explosion, *Y* axis on the right shows the excess velocity of the material that have been evaporated, *X* axis is the asteroid radius normalized altitude of detonation.

Note that, although the core of the model developed here is based on the radiation coupling model found in the work of Hammerling²², the numerical integration of Eq. (19) allowed us to perform a more general analysis of the nuclear option. For example, the optimal stand-off distance found by Hammerling *et al.* is $H = (\sqrt{2} - 1)R_s$, which is worked out by maximizing the sum of two fractions: the energy disposed over the asteroid against the total energy and the radiated surface against the total asteroid surface; whereas the optimal detonation distance in our model is much smaller ($H = 0.15R_a$), which is driven by an optimal combination of excess velocity and mass expelled due to the nuclear radiation.

As a final consideration on the model developed in this section, from Eqs. (18) and (19), we see that the total momentum change is dependent on the area radiated by the nuclear device and on the elevation angle. The radiated area and the elevation angles depend on the shape of the asteroid. If the asteroid is not

spherical but is an elongated body with the same mass, the worst case scenario is when the explosion occurs over the side of the asteroid with the smallest cross section area. In order to evaluate the loss of efficiency in the worst case scenario we computed the ratio between the total Δv for an elongated asteroid and the momentum change for a spherical asteroid with equal mass. Fig. 5 shows the Δv -ratio as a function of the elongation. Considering the typical measured elongation of known asteroids the maximum expected value is 2.5 for asteroid Geographos **, which corresponds to 18% reduction in the performance of the nuclear interceptor.

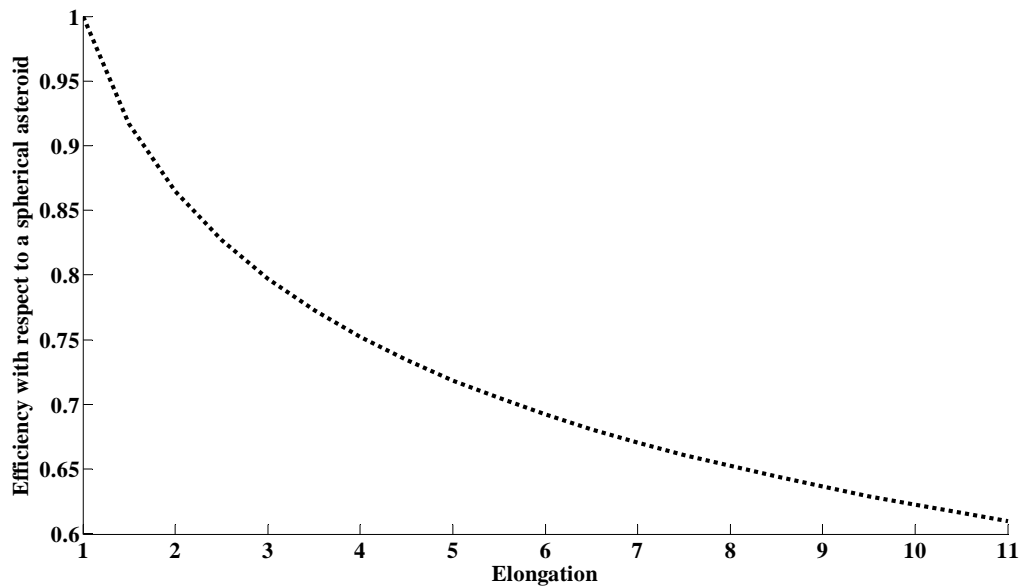


Fig. 5 Efficiency of the nuclear deflection for an elongated body. Nuclear detonation occurs over the side with the minimum cross-sectional area.

3. Spacecraft System Definition

Finally, it is assumed that a spacecraft is carrying a nuclear device with a mass $m_{wh} = 0.3m_d$. Fig. 3 shows the importance of maximizing the neutron radiation, therefore a fusion device is chosen as primary payload, since its fraction of nuclear radiation is considerably higher (see Table 1). The energy delivered by the explosion E_t can be computed as:

$$E_t = YTWm_{wh} \quad (21)$$

where YTW is the yield-to-weight ratio of a thermonuclear device. This parameter strongly depends on the mass of the nuclear device: the larger the mass, the higher the YTW ratio. We chose a ratio of 0.75

** http://echo.jpl.nasa.gov/~lance/nea_elongations.html

kTons/kg as a conservative option, although it ranges from 0.6 kTons/kg for a warhead of 165 kg to 2.25 kTons/kg for a warhead of 4000 kg^{††}.

B. Kinetic Impactor

The Kinetic Impactor is the simplest concept for asteroid hazard mitigation: the asteroid linear momentum is modified by ramming a mass into it. The impact is modeled as a simple inelastic collision resulting into a change in the velocity of the asteroid multiplied by a momentum enhancement factor¹¹. The enhancement is due to the blast of material expelled during the impact.

The value of the enhancement factor is extrapolated from cratering analysis, such as the one performed by K. A. Holsapple²⁵, and hypervelocity experiments. Both studies are Earth-based experiments on a small scale and its extrapolation to the asteroid size and conditions is difficult to quantify. A conservative value of 2 was chosen for all the analysis of this paper, however, for some asteroids with particular compositions and structures, the enhancement factor could be much larger¹¹. The variation of the velocity of the asteroid due to the impact is given by:

$$\delta \mathbf{v} = \beta \frac{m_i}{(M_a + m_i)} \Delta \mathbf{v}_{S/C} \quad (22)$$

where β is the momentum enhancement factor and $\Delta \mathbf{v}_{S/C}$ is the relative velocity of the spacecraft with respect to the asteroid at the deviation point.

C. Spacecraft Propulsion

A straightforward mitigation strategy could consist of a spacecraft landing on the asteroid and using its propulsion system to push the asteroid out of the impact trajectory. Either traditional chemical propulsion or low thrust propulsion systems could be used. Chemical propulsion provides very high thrust, but the excess velocity of the exhaust gasses is about ten times lower than that of the ionized plasma of low thrust propulsion systems, thus it requires much more propellant to achieve the same change in the linear momentum of the asteroid. For this reason a strategy based on a high thrust chemical engine was considered less efficient than a strategy with a low-thrust engine.

On the other hand, for electric propulsion (or low thrust approaches in general) the rotation of the asteroid becomes an issue. On a rotating asteroid the low-thrust system will not keep a constant pointing. The propulsion system will have to be switched on and off when the correct pointing occurs or the

^{††} <http://nuclearweaponarchive.org/>

asteroid rotation will have to be modified so that the propulsion system can be continuously active⁴. Another issue for such a mitigation approach is the definition of an appropriate attachment system between the propelling spacecraft and the asteroid. Finally, a problem pointed out by Scheeres et al.²⁶ is the formation of a transient atmosphere due to the surface operations: the combination of loose regolith and low gravity could result in a transient atmosphere of dust that could potentially affect the spacecraft mechanics and operations leading to contingencies.

Depending on how the thrust is applied and controlled we can subdivide the class of propulsion-based deflection methods into three subclasses: scheduled low-thrust, de-spin and push, precession and push.

In the following sections the scheduled low thrust model will be described in detail. The other possible low thrust techniques will be briefly outlined and then compared to the scheduled thrust option. For a detailed discussion of these alternative techniques the interested reader can refer to the work of Scheeres et al.⁴.

1. Scheduled Low Thrust Model

The scheduled thrust model assumes a mission in which two spacecraft land on opposite sides along the equator and thrust through the centre of mass of the asteroid. By properly scheduling the periods when the engines are switched on and off, we can obtain a quasi-constant thrust and a limited scattering factor. The scattering factor takes into account the misalignment from the optimal thrusting direction.

The total thrust of the system, i.e. the thrust of both engines together, is calculated using the following linear relationship:

$$T_n = m_{power} \frac{\xi}{\tau} \quad (23)$$

where m_{power} is the mass of the power subsystem, τ is the mass-to-power ratio and ξ is the specific thrust. The specific thrust ξ is set equal to 34 mN/kW which represents an average value for the most common ion thrusters²⁷. It is also assumed that the available power is generated by a subsystem with a mass which is 50% of the dry mass of the spacecraft, $m_{power}=m_d/2$, and capable of delivering 40 watts per kilogram ($\tau = 25 \text{ kg/kW}^{27}$).

The mass of the system at the asteroid m_i includes the propellant mass for the maneuver and the dry mass m_d of the spacecraft. Since the thrust of the propulsion system is fixed by the dry mass m_d and it will remain constant for the whole mission, the total impulse produced by the propulsion system on the asteroid can be computed as follows:

$$I_t = \int_{t_0}^{t_f} F dt = T_n \left(\frac{t_f - t_0}{2} \right) \quad (24)$$

where $F = T_n/2$ is the net force applied to the asteroid. Now, the total impulse can be computed using the variation in linear momentum produced by the ionized gas expelled from the propulsion system:

$$I_t = \int_{t_0}^{t_f} \frac{dm}{dt} v_e dt = (m_d - m_i) v_e \quad (25)$$

By combining Eqs. (23) – (25), we can obtain the dry mass m_d as a function of the initial mass m_i and of the duration of the pushing action $t_{push} = t_f - t_0$:

$$m_d = \frac{m_i}{\left[1 + \frac{\xi}{2\tau I_{sp} g_0} \frac{t_f - t_0}{2} \right]} \quad (26)$$

The maneuver could be as long as the time left before the asteroid impacts the Earth, although pushing for so long is not necessarily the best strategy. Since the dry mass depends not only on the initial mass, but on the duration of the deviation maneuver as well, see Eq. (26), it may be a better option to reduce the duration of the pushing maneuver to achieve a higher dry mass for a fixed initial mass, which translates into a better level of thrust.

An analysis of the achievable deviation as a function of the maneuver duration was carried out for six different asteroids from three different groups of NEOs: Apollo, Aten and Amor. Assuming a constant initial mass m_i for all the asteroids and a potential collision with the Earth in a range of 12 years, the achieved deviation was computed by numerically integrating Gauss' planetary equations over a variable pushing time.

As an example of the aforementioned analysis, Fig. 6, shows the total achieved deviation (right axis) and the total impulse (left axis) for a low-thrust deviation mission on asteroid Itokawa as a function of the percentage α of the total time available for applying the deviating action. The mass of the spacecraft at the beginning of the pushing action was assumed to be $m_i = 10000$ kg and the maximum available pushing time was fixed in this case to 10 years. The result in Fig. 6 shows how the maximum deviation is not achieved when the spacecraft is pushing for the whole available time before the collision. It is instead more convenient to use a higher thrust for a shorter time.

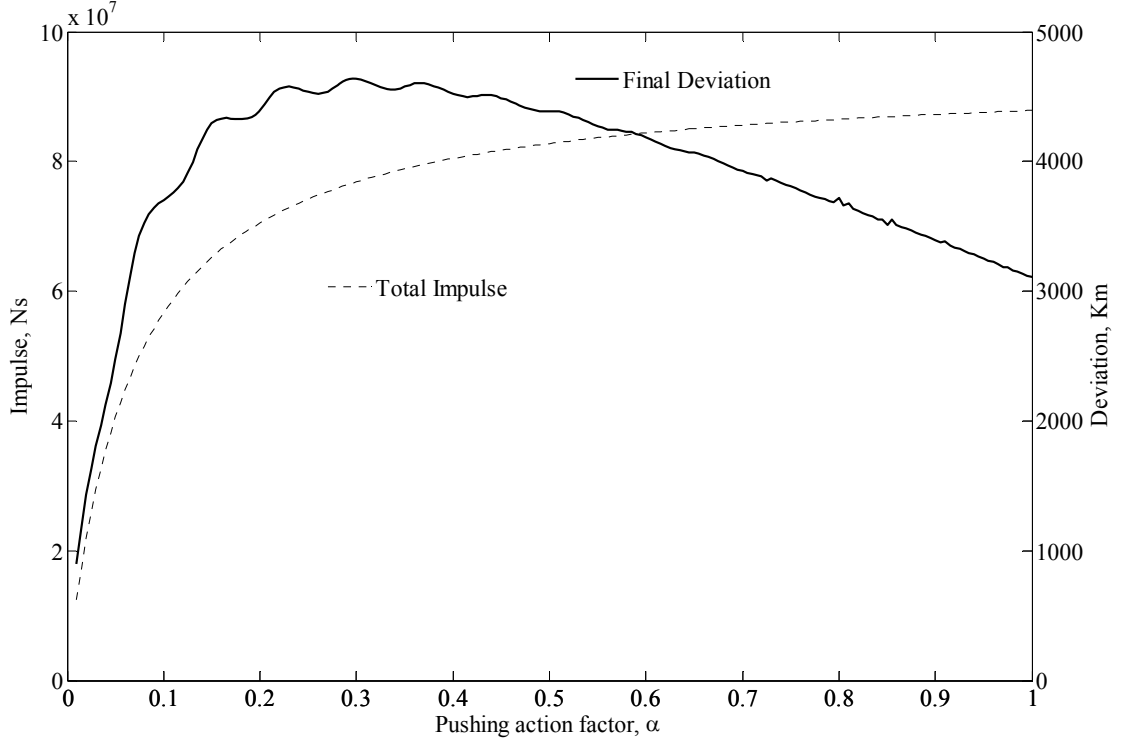


Fig. 6 Total impulse and deviation achieved for a varying α .

The result in Fig. 6 suggests a pushing maneuver that stops after the last perigee passage before 45% of the time between the arrival at the asteroid t_0 and the impact date. This prediction of the length of the pushing action matches the maximum deviation of the six studied cases with less than 2% error. Given the duration of the maneuver, the mass of propellant and the thrust can be calculated with Eq. (26).

2. Efficiency of the Scheduled Thrust

In order to measure the efficiency of the scheduled thrust, compared to a full continuous thrust directed along the optimal direction, we can define the *scattering factor*:

$$S_f = \frac{\int_0^{l_{rotation}} (\vec{F} \cdot \hat{v}) dt}{\int_0^{l_{rotation}} \vec{F}_{optim} dt} \quad (27)$$

where the integrations are along one complete asteroid rotation $l_{rotation}$, \hat{v} is the unit vector along the optimal thrusting direction, \vec{F} is the force vector delivered by the propulsion system landed on the asteroid and \vec{F}_{optim} is a force vector with equal modulus but always in the optimal direction \hat{v} .

If we assume that the asteroid is spinning much faster than it is orbiting around the Sun, we can define an asteroid orbit inertial reference frame and an asteroid equatorial inertial frame as shown in Fig. 7. In

the asteroid orbit frame, Fig. 7a, the angle ν is the angle between the orbital velocity and the \hat{x} axis, this angle will perform a complete rotation at every orbit. In the asteroid equatorial frame, Fig. 7b, the angle φ is the angle between the projection of the force vector on the $\hat{x}'\hat{y}'$ plane and the \hat{x}' axis. The angle φ will perform a full revolution at every rotation of the asteroid. The obliquity of the asteroid's equator ϕ is the rotation angle necessary to transform the asteroid's orbital inertial coordinates to the asteroid equatorial inertial coordinates. Eq. (27) can now be re-written as follows:

$$S_f(\nu, \phi, \varpi) = \frac{\int_{\varphi_0}^{\varphi_f} (|F| \hat{F}(\varphi, \varpi, \phi) \cdot \hat{v}(\nu)) d\varphi}{\int_0^{2\pi} |F| \hat{v}(\nu) d\varphi} \quad (28)$$

where the integration limits φ_0 and φ_f are chosen so that the scalar product $\hat{F} \cdot \hat{v}$ is positive in order to have a constant increase in the asteroid linear momentum.

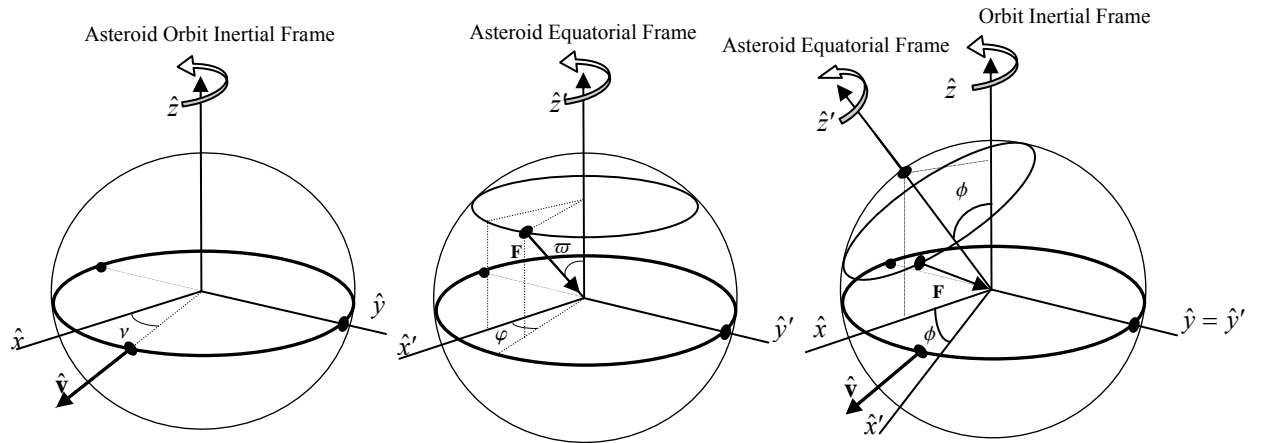


Fig. 7 a) Asteroid inertial orbital frame, b) asteroid equatorial inertial frame, c) a composition of both frames together on the right

Integrating Eq. (28) along a complete orbit, i.e., ν from 0 to 2π , and dividing by 2π , we obtain an average *scattering factor* that depends only on the obliquity of the asteroid and the complementary latitude ϖ of the landing site. Fig. 8 shows the *scattering factor* as a function of the obliquity angle ϕ and of the complementary latitude ϖ . The figure shows that for every obliquity it is always possible to choose a landing site that guarantees a *scattering factor* not lower than 0.3, which means that it is always possible to have at least 30% of efficiency of thrust without changing the rotational state of the asteroid. Note that this analysis does not depend on the asteroid shape but only on the obliquity of the asteroid's equator, thus the efficiency of the scheduled thrust would not be affected by the asteroid shape.

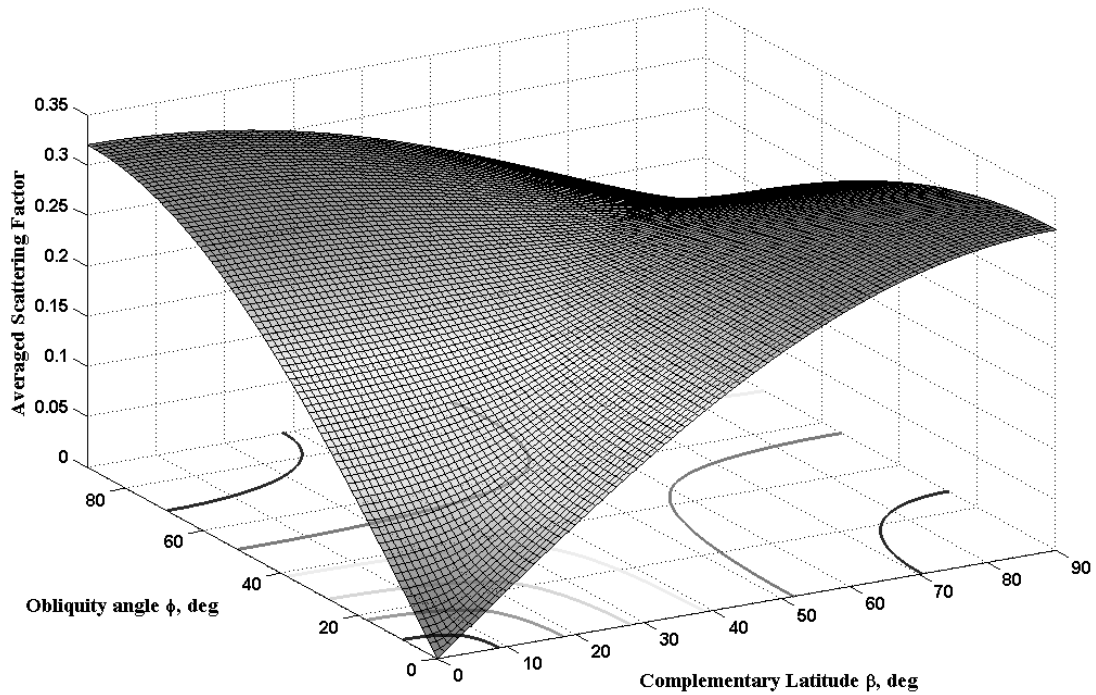


Fig. 8 Averaged scattering factor

3. Analysis of the Alternative Pushing Methods

Two alternatives have been suggested in order to solve the problem caused by the asteroid's rotation: asteroid de-spinning and simultaneous precession and push. Both techniques require a modification of the spinning rate of the asteroid. The de-spin method is a three phase method; during the first phase the low thrust propulsion is used to stop the rotation of the asteroid, next, a new rotational state is imposed in order to match the asteroid's orbital period, then the propulsion system is used to push the asteroid out of the collision trajectory. The second alternative requires one to re-orient the asteroid rotational pole and, as demonstrated by Scheeres et al.⁴, there is always an axial tilt such that it is possible to thrust continuously while maintaining a constant relative orientation between the rotational axis and the optimal thrusting direction.

Fig. 9 shows the effective total impulse produced by each one of the aforementioned techniques for a wide range of thrust levels. The effective total impulse for the scheduled thrust is the product of the thrust times the scattering factor times the pushing time. The effective total impulse for the despin method instead is the thrust times the available pushing time after the despinning operations. Finally the effective total impulse for the precession-push method is the product only of the thrust component in the direction of the asteroid velocity times the pushing time.

As it can be seen in Fig. 9, the de-spinning technique requires a minimum level of thrust in order to stop the rotation of the asteroid before the impact with the Earth. This minimum thrust level depends on the angular velocity of the asteroid's rotation and the time available for despinning and deviating the asteroid. For the analysis in Fig. 9, the maximum available time was set to 4 years for all the low-thrust methods.

Instead for the simultaneous precession and push, considering that the asteroid has already the proper configuration to start the deviating maneuver as soon as the spacecraft arrives, the faster the rotation is the higher the fraction of the thrust that goes into controlling the precession, hence less variation of the linear momentum for the same propellant consumption. In the remainder of this work, all analyses on the low-thrust propulsion method will consider only the scheduled approach, since, as Fig. 9 shows, the scheduled thrust method performs well for all the thrust levels, spinning rates and available pushing time considered in this study.

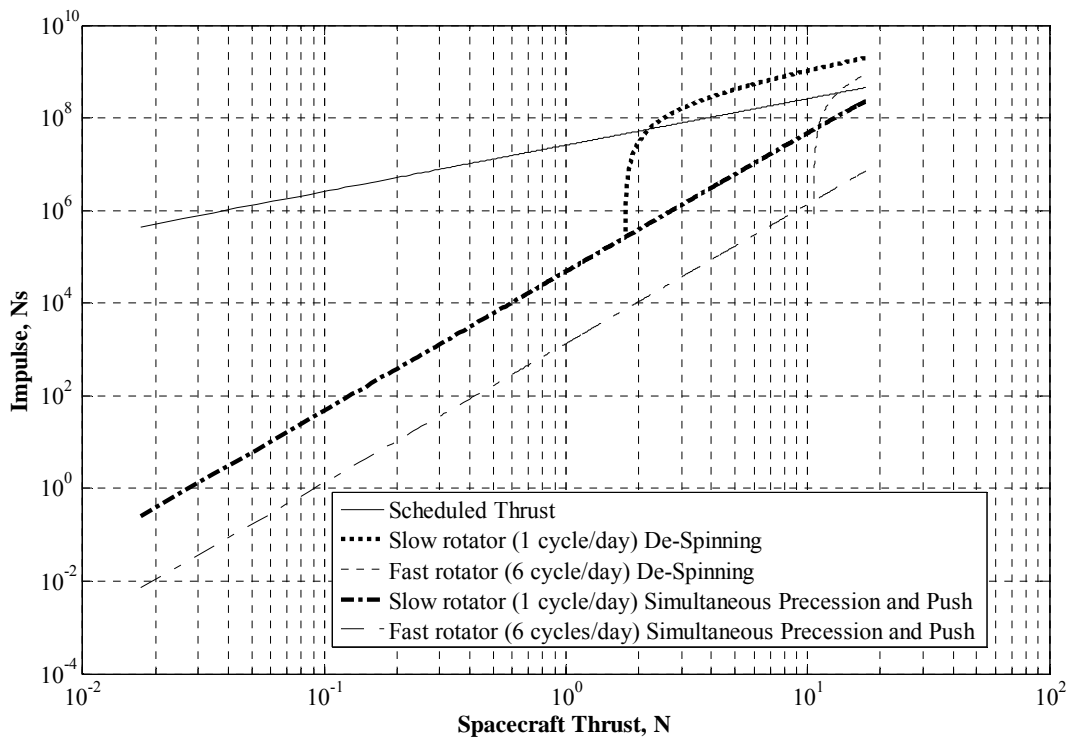


Fig. 9 Comparison among three possible low-thrust strategies for a wide range of thrust levels and 20 years of pushing time.

D. Mass Driver

The mass driver system generates a change in the velocity vector of the asteroid by shooting into space pieces of the asteroid outer crust. Some surface material is dug by a drilling device and accelerated

into space through an electromagnetic railgun. The advantage of this strategy is that the material used to change the linear momentum of the asteroid is obtained in situ and not carried from Earth.

1. Mass Driver Model

The model for the mass driver was developed assuming that a spacecraft with mass m_d is landed along the equator of the asteroid and directing the railgun along a line perpendicular to the rotation axis, which is assumed to be perpendicular to the velocity vector of the asteroid. Furthermore, it was assumed that when the railgun is not pointing in an optimal direction, the spacecraft is collecting material. The dug material is shot once per rotation when optimal pointing conditions are met, within a given tolerance.

The mass of the power subsystem was assumed to account for 30% of the dry mass m_d , which is in agreement with the results obtained by J. Olds²⁸. The mass-to-power ratio τ was set to 25 kg/kW²⁷, which is an averaged value for the power sources most commonly used in space. The energy efficiency of the railgun was set to 30%²⁹, hence approximately one third of the electrical energy generated by the power source is transformed into kinetic energy:

$$P_K = 0.3 \frac{m_{power}}{\tau} \quad (29)$$

where $m_{power} = 0.3 \cdot m_d$ is the mass of the power system and P_K is the total power converted into kinetic energy.

In the literature, a value of 100-300 m/s is suggested as a realistic excess velocity for the expelled mass^{28; 30}, therefore, in this paper, an excess velocity of 200 m/s, which is within the current technological capabilities²⁹, was considered for all the analysis. Given the excess velocity, the mass expelled per shot can be calculated with the following equation:

$$m_{launch} = \frac{2P_K \Delta t_{shooting}}{v_e^2} \quad (30)$$

where $\Delta t_{shooting}$ is time available to shoot the dug material into space, which was set equal to the time required to the pointing vector of the railgun to span a 10 degrees arc around the rotation axis of the asteroid, i.e., $\Delta t_{shooting} = 0.0278 T_{rot}$, where T_{rot} is the rotational period of the asteroid. It is assumed that power generated when the mass driver is not shooting (97% of the time) is sufficient for the mining system, e.g. a coring drill, to prepare the next projectile^{31; 32}.

The change in the velocity of the asteroid is determined by using the conservation of linear momentum and taking into account the change in the asteroid mass consequent to every shot:

$$\delta v = \frac{m_{\text{launch}}}{M_a(t)} v_e \quad (31)$$

At each impulsive δv there is a corresponding finite variation of the orbital elements of the asteroid and the new set of orbital parameters has to be calculated before the subsequent impulsive action.

Note that, similar to the low-thrust method, the mass driver generates a Δv only when the railguns point in the correct direction. The performance of this method, therefore, is not affected by the shape of the asteroid but by its rotational state.

E. Solar Collector

In 1993, Melosh et al. proposed the use of a mirror to focus the solar energy onto a small portion of the surface of the asteroid¹⁶. The resulting heat sublimates the surface material creating a jet of gas and dust that produces a continuous thrust. This thrust ultimately alters the orbit of the asteroid in a similar fashion to how a comet's orbit is altered by the expulsion of material from surface jets. A conceptually similar idea is to use a laser beam, either powered by a nuclear reactor or solar arrays, to induce the required sublimation of the surface material. In the following, a model is proposed to compute the deviating acceleration due to the flow of gases derived from the sublimation of the asteroid's surface. Although the model is applicable to both the solar collector idea and to the laser beam concept, the spacecraft model that will be employed in the following analyses assumes the use of a solar concentrator. This choice was motivated by the expected mass of the laser together with the power unit required to operate the laser: after a first estimation, the mass of a deployable mirror resulted to be smaller than the equivalent mass of the laser plus power unit. However, this does not intend to rule out the laser option; on the contrary, although, a more detailed spacecraft system analysis might demonstrate that the laser option is more advantageous than the solar collector, the sublimation model presented in this section and the following analysis will maintain their validity and the resulting conclusions would be applicable to the laser case as well as to the solar case.

1. *Spacecraft model*

It is assumed that the solar concentrator is made of a layer of reflecting material mounted on an inflatable supporting structure³³. The inflatable structure, together with the deployment system, attachments and related harnessing are assumed to account for 30% of the total dry mass of the spacecraft. From the work of John M. Hedgepeth^{33; 34} the mass-to-area ratio of the inflatable solar

concentrator is estimated to be 0.1 kg/m^2 . This is a conservative estimation when compared with the size and mass of space experiments such as Znamya and Echo balloons.

The size of the spacecraft is related to the amount of energy focused on the surface of the asteroid through the ratio between the area of the reflective surface and the area of the illuminated spot, or concentration ratio. Concentration ratios between 2000 and 3000 are possible for space solar concentrators³⁴. In the following, a concentration ratio of 2500 will be used, which is equivalent to a diameter for the illuminated spot 50 times smaller than the diameter of the mirror.

2. Thermal Model of an Asteroid

If a beam of light is focused onto the surface of the asteroid, the received power density can be calculated by using:

$$P_{solar} = \eta_{eff} \frac{S_{flux}}{r_{ji}^2} A_m (1 - albedo) \quad (32)$$

where A_m is the cross-section area of the reflective surface of the mirror, perpendicular to the direction of the solar radiation, A_s is the area of the illuminated surface on the asteroid, $\eta_{eff} = 90\%$ is the efficiency of the mirror assembly, $S_{flux} = 1367 \text{ W/m}^2$ is the solar flux at 1 AU, r_{ji} is the distance from the spacecraft to the Sun, which scales the solar flux, and the *albedo* was chosen as 0.2. This value approximates the albedo of a S-type asteroid, the surface of which is mostly composed of olivine. For the specific deviation method under investigation an albedo of 0.2 would correspond to a worst case scenario.

The time a portion of the surface spends under the spot beam is a function of the angular rotation of the asteroid and of the size of the spot, which is at the same time function of the size of the mirror and the concentration ratio. The model assumes the system to be an infinitely long rod, with the illuminated spot on one side of it. The illuminated surface is at a temperature of 1800 K, which is the sublimation temperature of forsterites²³. The long rod model represents a good approximation of the real system. In fact it can be proved that the conduction loss through the perimeter of this rod is much smaller than the energy loss due to the movement of the surface (i.e. asteroid rotation with a fixed beam).

Sublimation is due to the total absorbed energy. The net absorbed energy is the total energy focused on the surface minus the radiation and conduction losses. Energy loss due to conduction can be computed by first solving the differential equation for the surface temperature T ,

$$\frac{\partial^2 T}{\partial x^2} = \frac{c\rho_a}{\kappa} \frac{\partial T}{\partial t} \quad (33)$$

where c is the heat capacity (750 J/kg/K), ρ_a is the asteroid density, and κ is the thermal conductivity (2 W/m/K in this case). The thermal conductivity and heat capacity were calculated by using average values from different silicate materials on Earth, which are likely found on asteroids. Using the following initial and boundary conditions,

$$\begin{aligned} T(x, 0) &= T_0 = 278 \text{ K} \\ T(0, t) &= T_{subl} = 1800 \text{ K} \\ \lim_{x \rightarrow \infty} T(x, t) &= T_0 \end{aligned}$$

and applying a Laplace transformation, the above differential equation can be solved to give:

$$T(x, t) = T_0 + (T_{subl} - T_0) \cdot \operatorname{erfc} \left(\frac{x}{2 \sqrt{\frac{\kappa t}{c \rho_a}}} \right) \quad (34)$$

Finally, to calculate the conduction, the derivative of the temperature profile is calculated through a series expansion of the complementary error function, $\operatorname{erfc}(f(x))$. Therefore, with this model, the heat flux loss by conduction Q_{cond} on the surface of the asteroid ($x = 0$) can be calculated to be:

$$Q_{cond} = \frac{T_{subl} - T_0}{\sqrt{\frac{\pi t}{c \kappa \rho_a}}} \quad (35)$$

3. Rate of Expelled Mass

The heat generated by the sunlight will produce a flow of sublimated mass m_{exp} . Part of the energy goes into the sublimation process and part into the acceleration of the mass m_{exp} . The mass flow rate can be computed as:

$$E_v \frac{dm_{exp}(t)}{dt} = \Delta Q = P_{solar} - Q_{out} \quad (36)$$

where E_v is the enthalpy of sublimation, $dm_{exp}(t)/dt$ is the flow of sublimated mass and Q_{out} is the sum of the conduction heat loss Q_{cond} and the radiation heat loss Q_{rad} . The radiation heat loss Q_{rad} is defined according to the black body radiation formula as:

$$Q_{rad} = \sigma \varepsilon_{bb} T^4 \quad (37)$$

where σ is Stefan-Boltzmann constant, and ε_{bb} is the black body emissivity. By expanding the terms in Eq. (36) and solving for the mass flow, gives:

$$\frac{dm_{exp}}{dt} = \frac{1}{E_v} (P_{in} - Q_{rad} - Q_{cond}) \quad (38)$$

In order to calculate the total sublimated mass, Eq. (38) is integrated over the surface area under the illuminated spot. Note that, if the mass flow rate dm_{exp}/dt is negative, then there is not enough energy to sublimate the asteroid surface. Consequently, the limits of the integration have to be adjusted to avoid negative results. The horizontal surface position, x , and the illumination (or exposure) time can be related through the rotational velocity, V_{rot} , such that $x = V_{rot} \cdot t$ and $dx = V_{rot} \cdot dt$. Therefore, the integral can be rewritten in terms of the exposure time t , where the limits of the integration t_{in} and t_{out} are the times in which the asteroid surface moves inside and outside the illuminated spot respectively. Thus, the total mass flow is:

$$(\dot{m}_{exp})_{total} = 2V_{rot} \int_0^{y_{max}} \int_{t_{in}}^{t_{out}} \frac{1}{E_v} \left((P_{in} - Q_{rad}) - \left(\sqrt{\frac{ck\rho}{\pi}} (T_{subl} - T_0) \right) \sqrt{\frac{1}{t}} \right) dt dy \quad (39)$$

4. Total Induced Acceleration

Once the flow rate of evaporated material is computed, the average velocity of the particles is determined by using the Maxwell distribution for particles of an ideal gas:

$$\bar{v} = \sqrt{\frac{8kT_{subl}}{\pi M_m}} \quad (40)$$

where M_m is the mass of a single molecule of Mg_2SiO_4 and k the Boltzman constant.

The acceleration achieved by the asteroid due to the sublimation a_{solar} , can be calculated by dividing the thrust produced by the evaporation of the surface material and the remaining mass of the asteroid (the mass is decreasing due to the evaporation, e.g. for a 100-meter diameter mirror the mass flow rate is of the order of 1 kg/s, which for small asteroids can have a significant effect), corrected with a scattering factor S_{sc} accounting for the plume dispersion :

$$\|\mathbf{a}\| = \frac{(S_{sc} \cdot \bar{V} \cdot (\dot{m}_{exp})_{total})}{M_a(t)} \quad (41)$$

The scattering factor was computed assuming that the particles of debris and gas are accelerated uniformly over a semi-sphere, which corresponds to a 180 degrees plume cone. By integrating over the semi-sphere the effective components of the acceleration we get a value $S_{sc} = \frac{2}{\pi}$.

Fig. 10 shows the effects of the radiation and conduction heat losses, as well as the thrust for a 100 meter diameter mirror. In this simulation, the asteroid is assumed to have zero rotational velocity, but the exposure time varies between 0 and 30 seconds. As can be seen, below 10 seconds of exposure time the thrust level drops significantly.

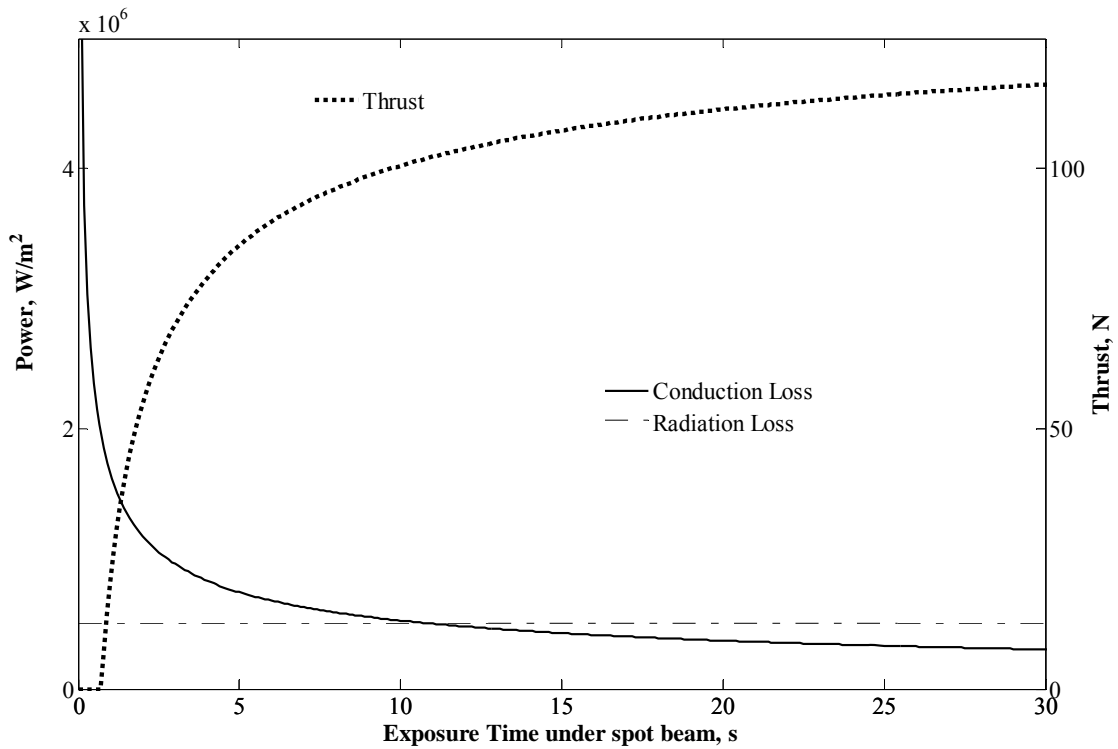


Fig. 10 Energy loss (left axis) and thrust (right axis) for a 100-meter diameter mirror.

5. Influence of the Asteroid Spinning Rate

As mentioned above, the exposure time, i.e., the time that the surface spends under the focused solar beam, depends strongly on the rotational speed of the asteroid. Fig. 11 shows the deviation achieved with a 60 meter mirror producing a deflection action on the asteroid Apophis. The deviation was computed by propagating Gauss' planetary equations for a period of two years with the deviating action aligned with the instantaneous velocity vector of the asteroid. As can be seen in the figure, as the rotation speed increases, the achievable deflection monotonically decreases.

At the light of the work of A. W. Harris³⁵, the most probable rotation state seems to be about 5.5 cycles/day. For this angular velocity, a mission with a 60 meter in diameter mirror would achieve a deviation of 14,000 km. Since the upper physical limit on the rotational speed is expected to be between 8 to 12 cycles/day³⁵, Fig. 11 shows that the deviation achieved with a solar collector, for any possible rotational state, would be at least 70% of the deviation achieved for a 5.5 cycles/day rotator. The upper limit on the rotational speed is assumed to be due to the rotational upper limit for asteroids without cohesive or tensile strength (i.e. rubble piles).

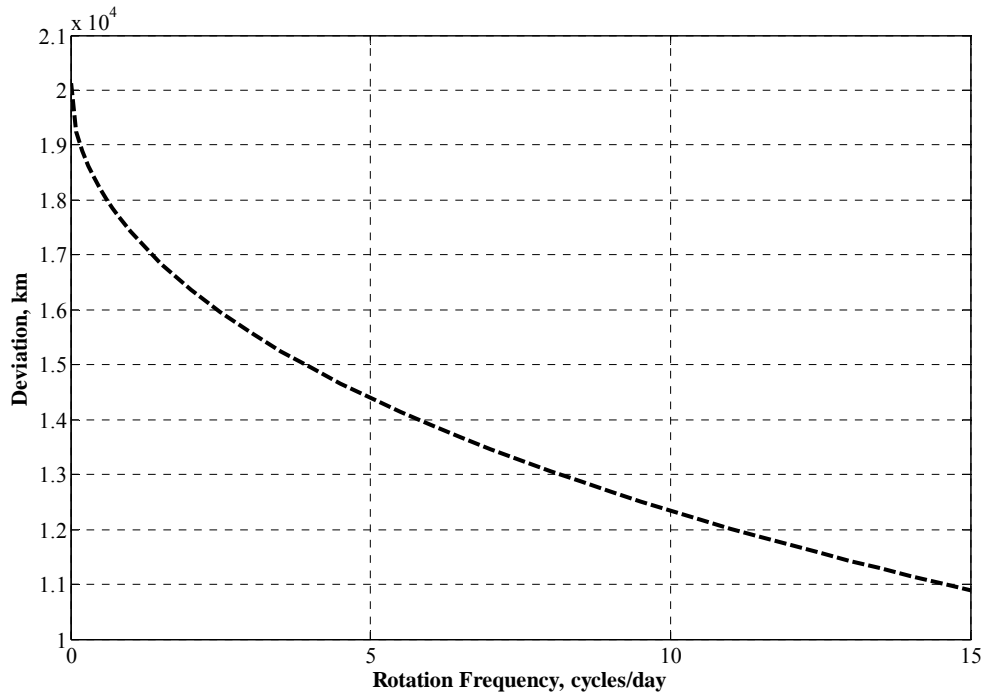


Fig. 11 Deviation as a function of the rotational speed produced by a 60 m diameter mirror acting on an Apophis-like asteroid during 2 years.

Finally, the elongation of the asteroid combined with its rotational state can affect the performance of this deflection method because the distance of the target spot on the surface of the asteroid from the mirror can vary with time. However, we can assume that the focal point of the mirror can be adjusted to cope with this variation. Adapting the focal point is a technological problem that does not affect the model presented in this section but is considered later in the paper when the Technology Readiness Level is taken into account. A first analysis of the problem related to focusing and pointing the light of the Sun, can be found in other works by the authors^{36; 37}. In the same works, there is a preliminary analysis of the control of the mirror in proximity of the asteroid.

F. Gravity Tractor

The gravity tractor exploits the mutual gravitational attraction between an asteroid and a spacecraft to pull the asteroid off its collision course with the Earth. In order to perturb the asteroid in the desired way, the spacecraft should maintain a constant hovering position during the pulling period. This concept was proposed by Lu & Love¹⁴ as a mean to modify the orbit of an asteroid, overcoming the uncertainties inherent into the asteroid surface composition, morphology and spinning rate.

1. System Definition & Architecture

The following hypotheses are used to develop the mathematical model of the gravity tractor:

- a. The power subsystem accounts for 50% of the dry mass m_d .
- b. The power subsystem is capable of delivering 40 watts per kilogram ($\tau = 25$ kg/kW).
- c. The propulsion subsystem generates 0.034 N/kW.

The total thrust of the spacecraft T_n is then computed by using Eq. (23). The closer the spacecraft hovers above the asteroid surface the bigger the gravity pull is. However, the exhaust gasses must not impinge on the asteroid surface, otherwise the centre of mass of the NEO-spacecraft system will remain unperturbed: in fact, it is the stream of mass escaping the system which generates a change in the linear momentum of the NEO³⁸. Note that, according to the action-reaction principle, using a specific amount of thrust to push the asteroid or using the same thrust to hover above it would lead to the same variation of the linear momentum, hence the same deviation. On the other hand, the thrusters must be properly pointed such that the cone of the exhaust gasses does not intersect the asteroid surface (see Fig. 12). As a consequence, the effective vertical thrust F_{hover} is always smaller than the total thrust T_n .

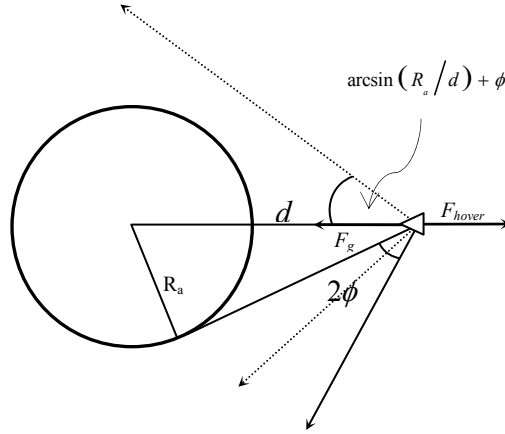


Fig. 12 Geometric diagram of the Gravity Tug and asteroid configuration.

As mentioned above, the thrusters have to be slanted laterally by an angle ϕ equal to half the angle of the exhaust cone in order to avoid the impingement of the propulsion gasses. With this configuration, the hovering distance can be calculated by solving the following system of equations:

$$\begin{aligned}
 F_{hover} &= T_n \cdot \cos\left(\arcsin\left(\frac{R_a}{d}\right) + \phi\right) \\
 F_g &= \frac{GM_a m_i}{d^2} \\
 F_{hover} &= F_g
 \end{aligned} \tag{42}$$

where F_g is the gravity attraction between spacecraft and asteroid, F_{hover} is the thrust force in the direction of the asteroid, ϕ is 20 degrees (in agreement with Lu & Love¹⁴), R_a is the mean radius of the

asteroid, G is the universal gravity constant, M_a is mass of the asteroid, m_i is the mass of the spacecraft at the beginning of the pulling maneuver and d is the hovering distance.

Since the spacecraft is consuming propellant to hold its hovering position, its mass will slowly decrease over time. The reduction in mass would allow the spacecraft to either hover closer to the surface or to reduce its thrust level while hovering at the same altitude. The latter option (i.e., keeping the hovering distance constant) is more advantageous since a reduction in the thrust leads to a lower propellant consumption, which in turn translates into a higher mass of the power subsystem for a fixed initial mass into space, which translates into a higher initial thrust and a lower hovering distance. By iterating this process, an optimal hovering point can be found that makes the constant altitude option more efficient than the variable altitude one.

If the constant altitude option is adopted, the mass of the spacecraft at any time t during the pulling maneuver can be computed assuming a mass consumption linearly proportional to the pulling action F_{hover} :

$$m(t) = m_i e^{-\left(\frac{GM_a(t-t_0)}{d^2 \cos\left(\arcsin\left(\frac{R_a}{d}\right) + \phi\right) I_{sp} g_0} \right)} \quad (43)$$

with the acceleration acting on the asteroid simply given by:

$$a_{gtug}(t) = \frac{Gm(t)}{d^2} \quad (44)$$

Therefore, the remaining mass m_d , at the end of a pulling maneuver with duration Δt_{tug} is:

$$m_d = m_i e^{-\left(\frac{GM_a \Delta t_{tug}}{d^2 \cdot \cos\left(\arcsin\left(\frac{R_a}{d}\right) + \phi\right) \cdot I_{sp} g_0} \right)} \quad (45)$$

and by using Eq. (45) in the system of equations (42), we obtain:

$$\frac{m_i e^{-\left(\frac{GM_a \Delta t_{tug}}{d^2 I_{sp} g_0 \cos\left(\arcsin\left(\frac{R_a}{d}\right) + \phi\right)} \right)}}{2} \frac{\xi}{\tau} \cos\left(\arcsin\left(\frac{R_a}{d}\right) + \phi\right) - \frac{GM_a m_i}{d^2} = 0 \quad (46)$$

which has to be solved to determine the hovering distance d .

Fig. 13 shows the total impulse provided by both, the Low Thrust and the Gravity Tug methods. Fig. 13 also shows the force over the asteroid produced by these two deviation methods. For a specific Low Thrust mitigation mission, the force is constant during the whole deviation maneuver, instead, for a

Gravity Tug mission the force decreases as a function of the mass of the spacecraft. It is interesting to note that, for pulling maneuvers longer than 13 years the force initially exerted by the Gravity Tug is higher than the force exerted by a low-thrust spacecraft with equal initial mass m_i . On the contrary, the total impulse is higher for the low-thrust method for deviation actions shorter than 135 years, the moment at which the total impulse provided by the Gravity Tug becomes higher than the one achieved by the Low Thrust.

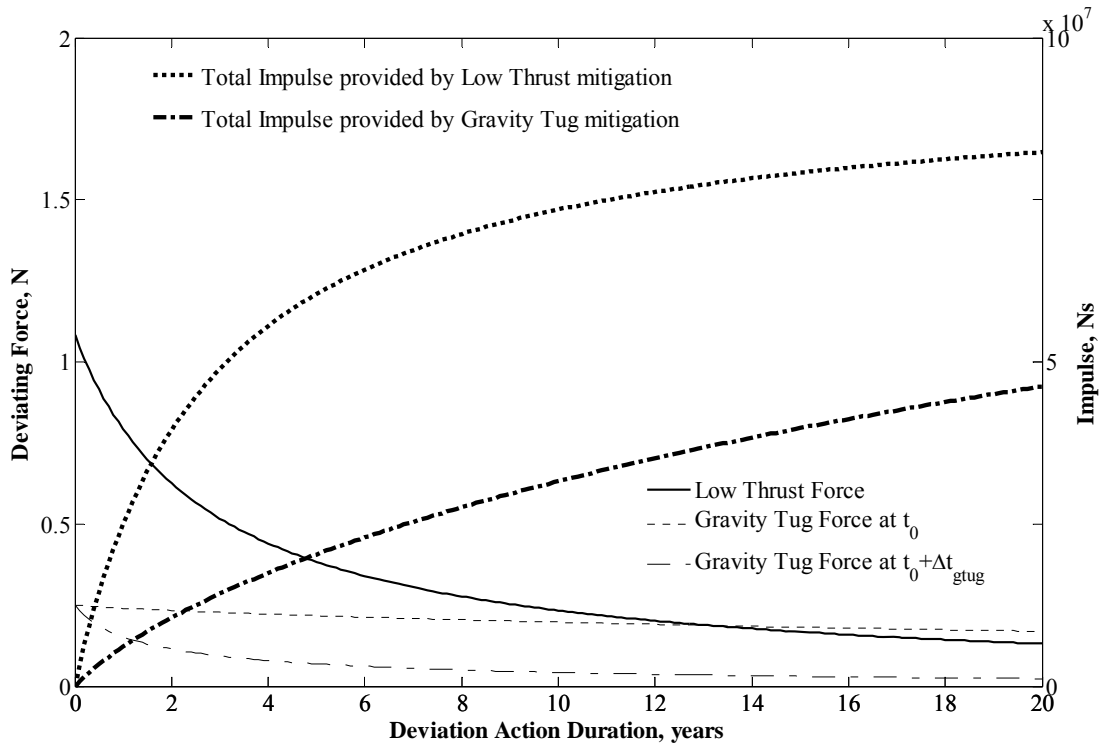


Fig. 13 Comparison between a Low Thrust mitigation mission and a Gravity Tug for a possible deviation of Apophis. Initial mass at asteroid arrival is 5000 kg for both methods.

Before concluding this section it is worth noting that the spacecraft has to hover at relatively close distance from the asteroid and maintain accurately its position and velocity. Since the shape and composition of the asteroid have an impact on its gravity field, the gravity tractor is not totally immune from the problems related to the unknown composition and morphology. Therefore, hovering control in a inhomogeneous gravity field generated by a non-spherical asteroid is an issue that has to be taken into account. However, a complete analysis of the effect of a non-spherical asteroid on the control of the gravity tug is out of the scopes of this paper and was already performed by other authors. The interested reader can refer to the work of Scheeres et al and Kawaguchi et al. for more details^{39; 40}.

IV. Multi-criteria Optimization Problem Formulation

The optimality of each strategy is here defined through a number of criteria or objectives that have to be attained. Unlike single objective problems, multiple objective problems look for a set of optimal values rather than a single optimal one. The general problem is to find a set X of feasible solutions \mathbf{x} such that the property $P(\mathbf{x})$ is true for all $\mathbf{x} \in X \subseteq D$:

$$X = \{\mathbf{x} \in D \mid P(\mathbf{x})\} \quad (47)$$

where the domain D is a hyper-rectangle defined by the upper and lower bounds on the components of the vector \mathbf{x} :

$$D = \{x_i \mid x_i \in [b_i^l, b_i^u] \subseteq \mathfrak{R}, i = 1, \dots, n\} \quad (48)$$

All the solutions satisfying property P are here defined to be optimal with respect to P or P -optimal and X can be said to be a P -optimal set. In the case of multi-objective optimization, if P is a dominance condition or Pareto optimality condition for the solution \mathbf{x} , then the solution is Pareto-optimal if $P(\mathbf{x})$ is true.

Each function vector j is associated to a scalar dominance index I_d such that:

$$I_d(\mathbf{x}_j) = \left| \left\{ i \mid i \in N_p \wedge \mathbf{x}_i \succ \mathbf{x}_j \right\} \right| \quad (49)$$

where the symbol $||$ is used to denote the cardinality of a set, \succ represents the dominance of the \mathbf{x}_i solution over the \mathbf{x}_j solution and N_p is the set of the indices of all the available feasible solutions. A solution vector \mathbf{x}_i dominates a solution vector \mathbf{x}_j when all the components of the criteria or objectives, vector $\mathbf{f}(\mathbf{x}_i)$ associated to \mathbf{x}_i are better (higher or lower) than all the components of the criteria vector $\mathbf{f}(\mathbf{x}_j)$ associated to \mathbf{x}_j . The property $P(\mathbf{x})$ in this case simply defines non-dominated solutions:

$$X = \{\mathbf{x} \in D \mid I_d(\mathbf{x}) = 0\} \quad (50)$$

The search for the P -optimal sets X , for each strategy, was performed through an agent-based search approach hybridized with a domain decomposition technique^{41, 42}.

G. Objective Function Definition

Three criteria or figures of merit were selected to define the optimality of each strategy:

- the warning time $t_w = t_{MOD} - t_l$, which is the interval between the launch date and the time at the point of closest approach; this figure of merit defines how far in advance we need to know

that an impact is going to occur, it gives a measure of our capability of quickly reacting to an incoming danger.

- the mass into space m_0 at departure, which is the mass of the spacecraft at the Earth, after launch; this figure of merit gives a measure of how difficult implementing a given strategy could be, if m_0 is not within our launch capabilities the difficulty of a given strategy increases.
- the total deviation Δr_{tot} at encounter calculated as $\Delta r_{tot} = \|\Delta \mathbf{r} + \delta \mathbf{r}\|$ where $\Delta \mathbf{r}$ is the vector distance of the asteroid from the Earth at the MOID point and $\delta \mathbf{r}$ is the variation given by the integration of Gauss' planetary equations (see Eq. (2)); this figure of merit, together with the mass into space, gives a measure of how easy deflecting an asteroid is with a given method. Note that we use the total deviation as figure of merit and not the ability of a particular deflection method to avoid the passage of the asteroid through dangerous key-holes⁴³. In this case even small $\delta \mathbf{r}$ would produce significant results, greatly enhancing the effectiveness of given deflection method.

The t_{MOID} is the date at which the asteroid reaches the point of Minimum Orbit Interception Distance from the Earth. Note that the Earth is not necessarily at that physical point in the orbit; the aim of this analysis is to measure the effectiveness and efficiency of each deviation method and not to reproduce a real impact scenario. In the following analyses, the t_{MOID} for each asteroid is the same for all the deflection strategies, and is kept fixed for all the simulations.

Table 3. Design Margins for the Spacecraft Mass

Strategies	m_0 margin
Solar Collector	25%
Electric Propulsion	25%
Mass Driver	25%
Gravity Tug	25%
Nuclear Interceptor	10%
Kinetic Impactor	5%

Even though the strategies were modeled with a very conservative approach, an additional margin on the mass into space m_0 was added in order to take into account the corrective maneuvers required during both the transfer leg and the deflecting arc. These margins, that can be found in Table 3, are also related, to some extent, to the maturity level of a given technology.

The criteria vector for a given method A is then defined as:

$$\mathbf{f}^A = \left[t_w^A, m_0^A, -\|\Delta \mathbf{r} + \delta \mathbf{r}\|^A \right]^T \quad (51)$$

where m_0 is augmented according to the design margin for method A. The problem is to find the set X of feasible solutions that are not dominated with respect to the criteria vector \mathbf{f}^A . Each solution corresponds to a mission leaving the Earth at a departure time t_0 , performing a transfer to the asteroid either along a Lambert's arc or a low-thrust spiral for a transfer time T and then applying the deviation action for a time t_{push} . For deviation strategies whose action is impulsive, such as kinetic impactor and nuclear interceptor, the transfer was modeled as a simple Lambert's arc. The velocity change at the Earth required to reach the asteroid was used to compute the propellant mass. For all the other deviation strategies, the transfer was modeled as a low-thrust spiral through a shape-based approach⁴⁴, assuming a departure from the Earth with zero relative velocity. The time t_{push} was set equal to the difference between the time at the point of closest approach and the time at interception, except for those strategies for which the model is providing an optimal value for t_{push} . All celestial bodies are considered to be point masses with no gravity and analytical ephemerides are used for the Earth and the asteroids. The general solution vector is defined as:

$$\mathbf{x} = [m_0, t_0, T, n_R, \lambda_{s1}, \lambda_{s2}]^T \quad (52)$$

where n_R is the number of revolutions of the Lambert's arc or of the low-thrust spiral and λ_{s1} and λ_{s2} are two shaping parameters for the low-thrust arcs. The search domain D is defined by the values in Table 4, therefore we looked, for each deflection method, for all the mission opportunities with a launch in the interval $[t_{\text{MOID}}-1000, t_{\text{MOID}}-7300]$ MJD2000 and a transfer time in the interval $[25, 1000]$ days. Note that the range of masses into space is pretty wide to account for a large variety of spacecraft designs, from microsattellites to multi-tons spacecraft. Note that the propellant mass required for the transfer is subtracted from m_0 when the spacecraft is at the asteroid. The residual mass, either m_i or m_d depending on the model, is then used to compute the deviation. All the missions that had a residual mass so low to produce a deviation close to zero were discarded and not included in the Pareto sets.

Table 4. Search domain for the multiobjective analysis

m_0	t_0	T	n_R	λ_{s1}	λ_{s2}
100	$t_{\text{MOID}}-7300$	25	0	-1	-1
100000	$t_{\text{MOID}}-1000$	1000	3	1	1

V. Results

A preliminary analysis was performed on the asteroid Apophis because of the potential impact with the Earth in 2036. Fig. 14 shows the Pareto optimal solutions found by the agent-based search for each

one of the deviation methods. Each solution shown in Fig. 14, each black dot, represents Pareto-optimal deviation mission to the asteroid Apophis, i.e. no other mission can be design, by changing the parameters in the solution vector in Eq. (52), that is improving all the three criteria at the same time.

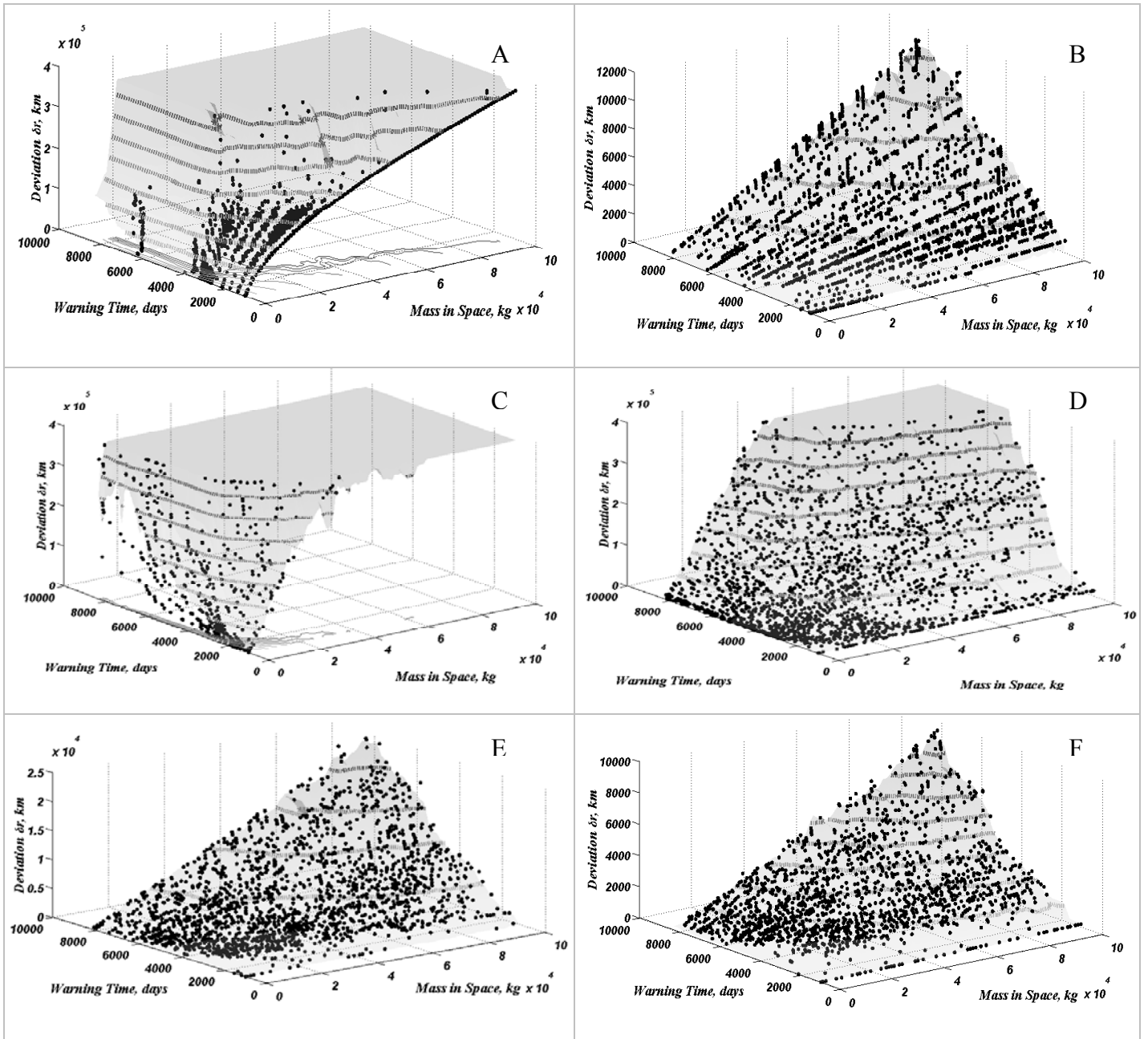


Fig. 14 Pareto sets for the six deviation methods applied to asteroid Apophis. A) Nuclear Interceptor. B) Kinetic Impactor. C) Solar Collector. D) Mass Driver. E) Low Thrust Propulsion. F) Gravity Tug.

Note that the range of warning times and mass into space are almost the same for all the six methods, while the range of the achieved deviation is substantially different. For example for the same mass into space and for the same warning time, the solar collector and nuclear interceptor are achieving a deviation

which is two orders of magnitude higher than the kinetic impactor. Furthermore, all strategies that employ a single impulse transfer present a characteristic striped distribution of the solutions mainly due to the periodicity of the optimal launch date. The direction of application of the deviating action, in fact, depends solely on the transfer and therefore an optimal launch date corresponds to a Pareto optimal solution.

The surfaces plotted in Fig. 14: A, C and D have a plateau at a deviation value of about 400,000 km. The plateau is due to the fact that the integration was stopped once the deviation reached one Earth-Moon distance. In order for the hypotheses behind the proximal motion equations to hold true, the variation of the orbit radius δr must be small compared to the unperturbed one. Therefore the Earth-Moon distance, was taken as upper threshold limit since this is considered to be sufficient to ward off the threat of an impact. The size of the plateau regions already suggests that both solar collector and nuclear interceptor provide similar performance. Note that the two approaches are utterly different, as the deviation is achieved through a continuous thrusting arc in the former case and through an impulsive change of the linear momentum in the latter.

H. Selected Asteroids

Although Apophis is an interesting study case, due to the threat that it poses to the Earth, additional case studies were considered in order to add comprehensiveness to this work. Instead of selecting more specific asteroids, it was decided to use the mean semimajor axis, eccentricity and inclination of two sets of 100 asteroids belonging to the Aten and Apollo groups. The asteroids in the sets, were taken from the list of the most dangerous ECA (Earth Crossing Asteroid) in the NASA's *NEO program* database^{**}. The angular Keplerian elements, Ω , ω and M_0 , were modified such that the MOID for a fixed collision date was minimal. Table 5 shows the Keplerian elements and t_{MOID} used in this study for Apophis and for the two additional virtual asteroids.

Table 5. Keplerian elements of the asteroids used in this study

	a (AU)	e	i (deg)	Ω (deg)	ω (deg)	M (deg)	$Epoch$ (MJD)	t_{MOID} (MJD)
Apophis	0.922	0.191	3.331	204.5	126.4	222.3	53800.5	62564.0
Aten-case	0.875	0.313	7.828	259.9	50.65	97.21	62481.0	62481.0
Apollo-case	1.706	0.518	10.70	266.8	121.2	18.09	62488.0	62488.0

^{**} <http://neo.jpl.nasa.gov/>

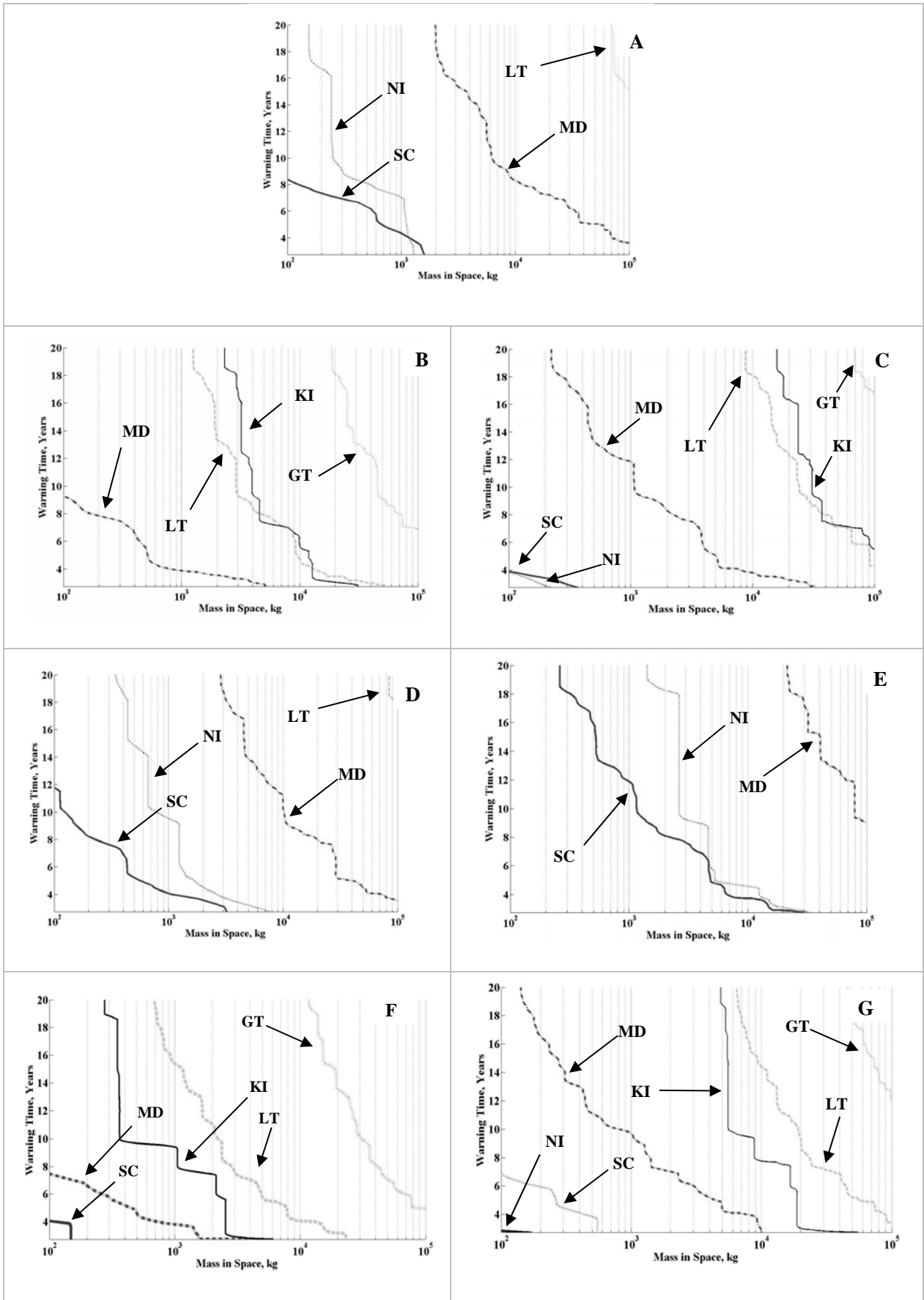
Apophis is assumed to have a mass of 4.6×10^{10} kg, which is equivalent to an asteroid with a diameter of 328 meters if a density of 2500 kg/m^3 and spherical shape are considered. The impact frequency of an object of this size is approximately 1 every 100,000 years¹. For the Aten and the Apollo cases, we considered masses ranging from 5.0×10^8 kg to 5.0×10^{11} kg (see Table 6 for a complete list of the cases analysed in this paper).

Table 6. Some physical characteristics of the asteroids used in this study and the approximated impact frequency

	M_a (kg)	Density (kg/m^3)	Diameter (m)	Estimated Impact Frequency	Rotation (hours)
Apophis	4.6×10^{10}	2500	328	1 every 100,000 years	30.54
Aten-1	5.0×10^8	2500	73	1 every 1,000 years	4.33
Aten-2	5.0×10^9	2500	156	1 every 10,000 years	4.33
Aten-3	5.0×10^{10}	2500	337	1 every 100,000 years	4.33
Aten-4	5.0×10^{11}	2500	726	1 every 1,000,000 years	4.33
Apollo-1	5.0×10^8	2500	73	1 every 1,000 years	4.33
Apollo-2	5.0×10^9	2500	156	1 every 10,000 years	4.33
Apollo-3	5.0×10^{10}	2500	337	1 every 100,000 years	4.33
Apollo-4	5.0×10^{11}	2500	726	1 every 1,000,000 years	4.33

I. Pareto Contour Lines

A simple way to compare the 3D Pareto fronts of the different strategies and asteroids is by plotting deviation isolines. Fig. 14 shows the isolines for a deviation of 13720km for each deviation strategy and each case studied. This deviation was calculated taking into account the deflection of the trajectory of Apophis due to the gravity attraction of the Earth at its final approach and correcting a distance of 1 Earth radius with a hyperbolic factor that depends on the relative velocity between the Earth and the threatening object⁴. The deflection isoline of 13720km is used in all the plots in Fig. 14 to facilitate the comparison between the different asteroids, despite the fact that for our Aten and Apollo cases the hyperbolic corrected distance would be lower since the relative velocities of those at encounter with the Earth are higher than the Apophis relative velocity, therefore they should be less affected by the Earth gravity.



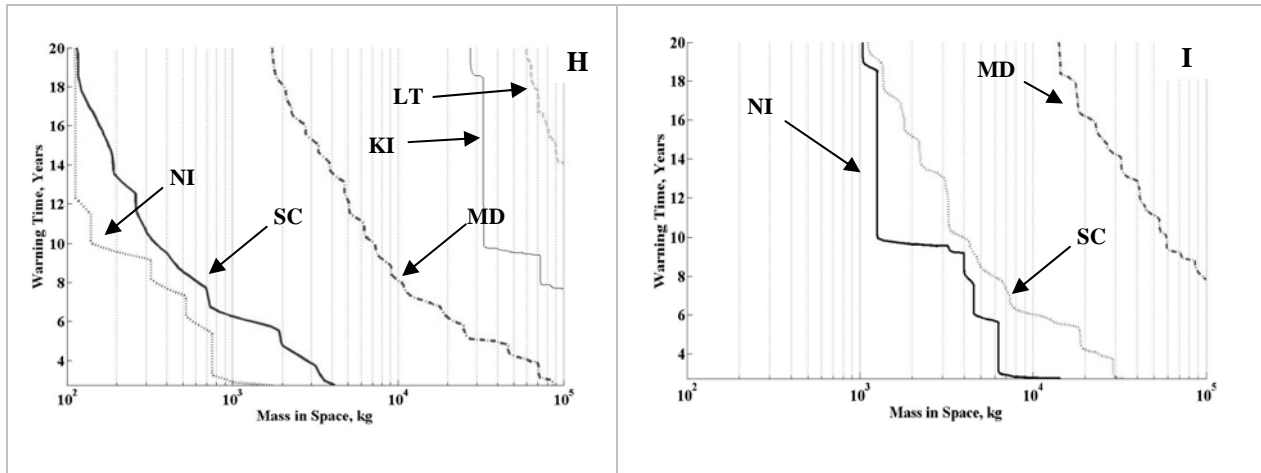


Fig. 15 Pareto front contour lines for a deviation of 13720 km for all the analyzed deviation methods; solar collector (SC), low thrust (LT), mass driver (MD), nuclear interceptor (NI), kinetic impactor (KI), gravity tug (GT). Each figure is for a different mass of the asteroid: A) Apophis case, B) Aten-1 case, C) Aten-2 case, D) Aten-3 case, E) Aten-4 case, F) Apollo-1 case, G) Apollo-2 case, H) Apollo-3 case, I) Apollo-4 case

In the three cases with mass of the order of 5×10^{10} kg (i.e., Apophis, Aten-3 and Apollo-3) only three strategies, namely the mass driver, the nuclear interceptor and the solar collector, yield the desired deviation with a mass in space smaller than 100,000 kg and a warning time shorter than 10 years. The low thrust method is also able to provide 13720km deflection, but only with a mass in space close to 100,000kg and 20 years of warning time.

The kinetic impactor is remarkably close to the low-thrust in the Aten cases (Fig. 15 B and C) especially for short warning times, and in the Apollo cases (Fig. 15 F, G and H) not only it clearly outperforms the low-thrust strategy, but its efficiency increases almost ten-fold when compare with the Aten case. The main reason for this high efficiency of the kinetic impactor in the Apollo cases is due to the fact that being the Apollo the asteroid with higher eccentricity and inclination, thus higher relative velocity with respect the orbit of the earth, a high speed impact is less expensive, in terms of propellant mass, than in the Aten cases and more mass-efficient than a rendezvous.

It is worth to underline that for small asteroids (Fig. 15 B, C, F and G) simple methods like the kinetic impactor are able to provide the required deviation with a relatively small mass in space. On the other hand, for larger asteroids (Fig. 15 E and I), only the three more efficient methods are able to provide the required deviation within the given range of mass into space and warning time.

J. Strategy Comparison

The effectiveness and efficiency of each strategy are expressed through a set of Pareto optimal points (e.g., Fig. 14). In order to compare one strategy against the others it is possible to use the concept of dominance of one Pareto set over another: an element (or solution belonging to the Pareto set) i of strategy A is said to be dominated by element j of strategy B if all the components of the vector objective function \mathbf{f}_j^B are better (i.e., t_w and m_0 smaller and $\|\Delta r + \delta r\|$ bigger) than all the components of the vector objective function \mathbf{f}_i^A . Then, the dominance index $I_i(m_A)$ of an element i of strategy A with respect to strategy B is the cardinality of the set of elements of the Pareto-optimal set of strategy B that dominate element i :

$$I_i(m_A) = \left| \left\{ j \mid \mathbf{f}_i^A \prec \mathbf{f}_j^B \right\} \right| \quad (53)$$

where the dominance symbol \prec in Eq.(53) means that \mathbf{f}_j^B dominates \mathbf{f}_i^A , i.e. all the components of \mathbf{f}_j^B are better than all the components of \mathbf{f}_i^A . Thus if the value of the dominance index of the element i is 0, it means that there is no solution in the Pareto-optimal set of strategy B that has all the three criteria that are better than the three criteria associated to element i . We can now say that strategy A dominates strategy B if the percentage of the elements of A that are dominated by B , i.e. the percentage of elements of A with dominance index $I(m_A)$ different from 0, is less than that of the elements of B that are dominated by A :

$$d_i(m_A) = \begin{cases} 1 & \text{if } I_i(m_A) > 0 \\ 0 & \text{if } I_i(m_A) = 0 \end{cases} \quad (54)$$

$$m_A \succ m_B \Rightarrow \frac{1}{N_A} \sum_{i=1}^{N_A} d_i(m_A) < \frac{1}{N_B} \sum_{j=1}^{N_B} d_j(m_B)$$

where N_A is the total number of the solutions in the Pareto set of method (or strategy) m_A and N_B is the total number of solutions in the Pareto set of method (or strategy) m_B .

Table 7, Table 8 and Table 9 show the dominance of the different strategies applied to Apophis, Aten-3 and Apollo-1 (i.e., three cases with similar mass). The numbers in the tables are the percentage of elements of the method in the corresponding row that dominate over the elements of the method in the corresponding column. For example, if we look at Table 7, 100% of the solutions in the Pareto set of the Mass Driver dominate (i.e. all the three criteria are better) the solutions in the Pareto set of the Low Thrust. Note that the numbers in every column do not add up to 100 with the corresponding numbers in every row. For example, for Apophis (see Table 7) 14% of the Kinetic Impactor solutions are dominant over Low-thrust solutions while 98% of Low-Thrust solutions are dominant over Kinetic Impactor solutions. The reason for that is that we compute the percentage of points within each Pareto set, therefore

it could well be that 100% of the points of a set are dominating only a small fraction of the points of another set.

Table 7. Strategy Dominance for Apophis

	Solar Collector	Low Thrust	Mass Driver	Nuclear I.	Kinetic I.	Gravity Tug
Solar Collector		100	100	95	100	100
Low Thrust	0		0	0	98	100
Mass Driver	0	100		0	100	100
Nuclear Interceptor	5	100	100		100	100
Kinetic Impactor	0	14	0	0		100
Gravity Tug	0	0	0	0	2	

Table 8. Strategy Dominance for Atens-3

	Solar Collector	Low Thrust	Mass Driver	Nuclear I.	Kinetic I.	Gravity Tug
Solar Collector		100	100	95	100	100
Low Thrust	0		0	0	88	100
Mass Driver	0	100		0	100	100
Nuclear Interceptor	8	100	100		100	100
Kinetic Impactor	0	42	0	0		100
Gravity Tug	0	0	0	0	1	

Table 9. Strategy Dominance for Apollo-1

	Solar Collector	Low Thrust	Mass Driver	Nuclear I.	Kinetic I.	Gravity Tug
Solar Collector		100	100	14	100	100
Low Thrust	0		0	0	0	100
Mass Driver	0	100		0	100	100
Nuclear Interceptor	97	100	100		100	100
Kinetic Impactor	0	100	0	0		100
Gravity Tug	0	0	0	0	0	

From the dominance comparison, the solar collector and nuclear interceptor result to be the dominant methods in the studied domain. Solar collector achieves better performance than nuclear interceptor for the Atens class, but not for the Apollo class. This is due mainly to the fact that the smaller semimajor axis of the Atens group means better solar radiation and therefore higher efficiency of the solar collector. It is interesting to underline that the Kinetic Impactor dominates the Low Thrust option for the Apollo case. The same result can be seen in Fig. 15, though limited to one particular value of deflection δr .

Though, as shown in Fig. 15, for small size asteroids, techniques such as Kinetic Impactor and Gravity tug become effective, the relative performance difference between two deflection strategies does not change, therefore here we report only three sample tables for the dominance evaluation. Furthermore, it should be noted, that due to the stochastic nature of the search for Pareto optimal solutions performed

by the optimizer, the curves in Fig. 15 can locally change if the optimizer is run several times. As a consequence, also the dominance evaluation is subject to minor changes (few percentage points).

VI. Influence of the Technology Readiness Level

As an additional criterion, we considered the technology readiness level (*TRL*) of each method as a measure of its expected viability in the near future. We assumed that in the case of an impact the required time to implement a given deviation method had to take into account the necessary development effort and that the development effort was driven by the piece of technology, composing the deviation method, with the lowest *TRL*. In the following, the development effort will be measured in man years (amount of work performed by an average worker in one year). Although this is not an exact measure of the time required to implement a given technology, it gives a good estimation of the added difficulty to bring a given technology to full operation capability. The actual development time depends on the amount of available resources and on political considerations that are out of the scopes of this paper. Therefore, we assume that the development effort is a measure of the required delay in the implementation of a given deflection method. To be more precise, the warning time is redefined to be the time between the point when a given technology starts to be developed and the predicted impact time. For example, given a technology we need a man-time Δt_{dev} to bring that technology to a sufficient level of development to be launched, therefore the warning time becomes $t_w = t_{MOID} - t_l + \Delta t_{dev}$. We use a standard definition of *TRL*^{45; 46}, as summarized in Table 10, we assume no limitations due to economic or political issues, and no developments driven by other applications or breakthrough discoveries. Therefore, we assign the current *TRL* to each of the deviation methods and we assume that the *TRL* will remain constant till $t_{MOID} - t_w$. These assumptions correspond to a situation in which cost is not an issue in case a global threat has to be faced, but, on the other hand, both economic and political issues prevent any development not motivated by a confirmed impact.

Table 10. Technology Readiness Levels.

TRL	Technology Readiness
1	Basic principles observed and reported
2	Technology concept and/or application formulated
3	Analytical & experimental critical function and/or characteristic proof-of-concept
4	Component and/or breadboard validation in laboratory environment
5	Component and/or breadboard validation in relevant environment
6	System/subsystem model or prototype demonstration in a relevant environment (ground or space)
7	System prototype demonstration in a space environment
8	Actual system completed and "Flight qualified" through test and demonstration (ground or space)

The *TRL* of each deviation methodology was determined taking into account past missions and scientific research up to date. The *TRL* for each method was mapped into the number of man-years Δt_{dev} , for increasing a given technology from the current *TRL* to *TRL* 9, through the logistic function:

$$t_{dev} = \frac{a}{1 + e^{-\frac{\Lambda - t_c}{\tau}}} + b \quad (55)$$

where t_{dev} is the required development effort (measured in man years) to bring a technology from *TRL* 1 to *TRL* Λ . The parameter t_c represents a turning point for the development of a technology when the critical function characteristics have been already demonstrated experimentally and analytically but the components have not yet been tested in a relevant environment. Around that point, we expect a maximum increase in the investments to turn a conceptual design into a first hardware prototype. In the following we set $t_c=5$ which is a value corresponding to *TRL*5. The coefficients a , b , and τ were chosen so that:

$$\begin{aligned} t_{dev}(\Lambda = 2) &= 0; \\ t_{dev}(\Lambda = 9) &= 15; \\ t_{dev}(\Lambda = 7) - t_{dev}(\Lambda = 4) &= 10 \end{aligned} \quad (56)$$

The set of boundary conditions in Eq.(56) corresponds to a maximum development effort of 15 man-years from *TRL* 2 to *TRL* 9 and a development effort from breadboard to first prototype system demonstration into space of 10 man-years. The resulting Δt_{dev} is simply the difference between the t_{dev} at *TRL* 9 and the t_{dev} at a given *TRL* Λ (see Fig. 16).

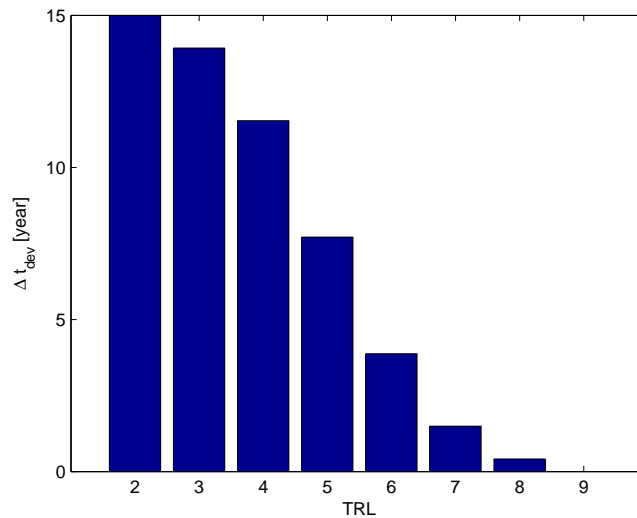


Fig. 16. TRL mapping into required development effort to reach full operational capabilities

Note that we start with a minimum *TRL* of 2 since the basic concept and the application have been already formulated for all the deflection methods. Then, in the assignment of *TRL* to each deflection method we will distinguish between innovate technologies pre or during mission assessment phase (*TRL* 1 to 4) and existing technologies during mission definition phase (*TRL* 5 to 9).

K. TRL Assignment

In this section, we assign a *TRL* to each one of the deflection methods. Each deviation method is characterized by a number of critical technologies that need to be developed in order make the method actually feasible. The technologies considered in this analysis are only strictly related to each model of deflection method presented above and do not include the development of new launch capabilities and the required increase in the knowledge of the physical and orbital characteristics of the asteroids. Once the critical technologies are identified and a *TRL* is assigned to each of them we assign to the whole deflection method the *TRL* of the least developed technology. Since the *TRL* for some methods is uncertain, due to several concurrent factors, we assign to each deflection method an interval of *TRLs*. These intervals represent our level of confidence in the present level of development of a given technology. The assignment is based on Table 10 and on the assumption that a technology at *TRL* 9 that is reused in a new application with new requirements needs to be downgraded to *TRL* 4.

1. Kinetic Impactor

Although the kinetic impactor strategy has not been completely proven yet, a mission with similar characteristics, Deep Impact, was already successfully flown. Furthermore, although the impact velocity is a critical issue for this strategy, the average impact velocity of all solutions found in this study was 10 km/s, which is indeed very similar to the Deep Impact crash velocity (~ 10.2 km/s). For this deflection method, we consider two critical issues: high precision targeting, enhancement factor. The former issue would require a better knowledge of the motion of the centre of mass and rotational state of the asteroid in order to correctly hit the asteroid and transfer the required Δv , the latter issue would required a better knowledge of the composition and morphology of the asteroid. Thus, both cases are related to an increased knowledge of the characteristics of the asteroid. The former issue would also require the development of accurate navigation and orbit determination capabilities for fast close encounters. However, we can assume that this technology is already available and at *TRL* 9 given all the past and

present missions using gravity assist maneuvers. Since only one example of high velocity impact exists, we assign a *TRL* ranging between 7 and 8 to the kinetic impactor.

2. *Nuclear Interceptor*

Nuclear weapons have not been tested in space since the *Limited Test Ban Treaty* forbids all nuclear use in both space and atmosphere. Furthermore, although the effects of a nuclear explosion can be considered to be well known, there has not been any Nuclear Interceptor prototype or any equivalent prototype in space, therefore the *TRL* should be no higher than 6. On the other hand the launch of nuclear warhead is fully developed, thus we assign a *TRL* ranging from 6 to 8.

3. *Low Thrust*

Low Thrust requires the following main critical technologies: low-thrust propulsion, nuclear power generation, autonomous rendezvous and landing, anchoring system. Low-thrust engines delivering the required level of thrust have been used as main propulsion systems since 1998, with Deep Space 1 therefore they can be considered at *TRL 8* already. On the other hand, some missions in the Pareto set require a thrusting time of more than 1000 days, which exceeds the operational lifetime of current electric engines. For those missions either a complete redesign of the propulsion system or multiple engines would be required, in the former case the *TRL* would be not higher than 4. Rendezvous and landing operations for small spacecraft can be considered at *TRL 7* due to previous and ongoing missions to comets and asteroids (such as Rosetta⁴⁷ and Hayabusa⁴⁰). Nuclear reactors delivering between 1 to 10 kW have already flown since 1965 (e.g. the US SNAP-10A) and higher power reactors can be derived from terrestrial ones with limited new developments, thus this technology can be considered between *TRL 6* and *7*. An anchoring system was already designed for the lander of Rosetta though for more massive spacecraft the anchoring and landing system would require further development therefore their *TRL* can not be considered higher than 6. Therefore, overall, the *TRL* for the Low Thrust method can be considered ranging from 4 to 6.

4. *Gravity Tug*

Gravity Tug requires the following main critical technologies: autonomous proximal motion control in an inhomogeneous gravity field, nuclear power generation, low-thrust propulsion. A hovering approach to the asteroid Itokawa was used by the mission Hayabusa and the same technique is proposed for the gravitational tug, but to a completely different level of accuracy and autonomy, therefore its *TRL* should be between 3 (no test in relevant environment) and 5 (if Hayabusa is considered to be an example of

hovering in relevant environment). Low-thrust propulsion has the same *TRL* as for Low-Thrust deviation methods and share the same issues, in particular the operational lifetime since the number of missions with a pushing time higher than 1000 days is higher than for the Low-Thrust. Nuclear power generation for this method has the same *TRL* as for the Low-Thrust technique therefore the overall *TRL* for the Gravity Tag ranges from 3 to 5.

5. *Mass Driver*

Mass Driver requires the following main critical technologies: autonomous rendezvous and landing, autonomous mining in microgravity, high power railgun system, nuclear power generation, anchoring system. Magnetic railgun systems have already been developed and used on Earth for other applications²⁹, therefore we can assume a *TRL* 5, rendezvous and landing is *TRL* 7 as for other methods as well as nuclear power. The anchoring system and the mining system in microgravity instead require a substantial development^{31-32; 48-49}, thus their *TRL* is no higher than 4. Though drilling systems have been already tested in space, the level of power involved in a successful implementation of the Mass Driver would require a substantial redesign of the mining and anchoring system to cope with the microgravity conditions. Since a conceptual design for this technology already exists¹⁷ (*TRL* 2) we can assign a *TRL* ranging between 2 and 4 to the Mass Driver.

6. *Solar Collector*

Solar Collector requires the following main critical technologies: adaptive optics, deployment and control of ultra-light mirrors, autonomous orbit control, accurate autonomous pointing. The mirrors have to focus the light of the Sun in every operational conditions and therefore the curvature has to be actively controlled, furthermore it is expected that the light is collimated by a series of lenses. The collimation of the beams is of primary importance to maintain the required power density, especially for rotating asteroids with high elongation, for which the closest and farthest distance from the spacecraft could be considerable. Adaptive optics for terrestrial⁵⁰ and space applications have been developed and used in space on telescopes and therefore their *TRL* could be 7, on the other hand it is required to have an autonomous control of the pointing and of the focusing dependent on the power density of the illuminated spot. This would require a substantial redesign and a new development, therefore the *TRL* is between 2 and 3. The deployment of ultra-light structures of small to medium dimensions has already been tested in space and would be between *TRL* 6 and 7⁵¹ and ultra-light adaptive mirrors for space have already been developed and prototyped and would be between *TRL* 4 and 5^{52; 53}, on the other hand the deployment and

control of large focusing mirrors is still at a conceptual stage and therefore at *TRL* 2. Accurate autonomous orbit control is at the same level of the Gravity Tug and therefore is at *TRL* 4. Therefore, the overall *TRL* for the Solar Collector is between 2 and 3.

Table 11. TRL for all the deviation methods

Deviation Method	TRL intervals
Kinetic Impactor	7-8
Nuclear Inceptor	6-8
Low-Thrust Gravity Tug	4-6
Mass Driver	3-5
Solar Concentrator	2-4
	2-3

The *TRL* intervals for each deviation methods are summarized in Table 11 and were translated into a Δt_{dev} according to Fig. 16. The development time due to the technology readiness level is applied to the Pareto optimal sets by extending the warning time t_w :

$$\mathbf{f} = [t_w + \Delta t_{dev}, m_0, -\|\Delta r + \delta r\|]^T \quad (57)$$

Since the impact date is kept fixed for all the strategies, all the Pareto optimal solutions that would require a warning time such that the arrival date at the asteroid exceeds the t_{MOID} are removed from the comparison. As a consequence, a strategy with a low technology readiness would require a longer warning time for the same deviation or a lower deviation for the same warning time. Table 12 shows the intervals of dominance of all the strategies for a simulated deviation of Apophis after applying the range of *TRL* from Table 11.

Table 12. Apophis TRL Comparison Table (a=0.92 A.U.).

	Solar Collector	Low Thrust	Mass Driver	Nuclear I.	Kinetic I.	Gravity Tug
Solar Collector		100	100	6-17	100	100
Low Thrust	9-52		9-39	0	0-86	100
Mass Driver	0-22	99-100		0	99	99-100
Nuclear Interceptor	100	100	100		100	100
Kinetic Impactor	76-68	100-45	79-63	10-0		100
Gravity Tug	25-22	1-0	25-5	0	0	

By comparing Table 12 with Table 7, few preliminary considerations can be drawn. The first is that when the Technology Readiness Level is considered, the kinetic impactor becomes competitive since its Pareto front encloses parts of the criteria space that the other strategies are not able to cover. On the other

hand, even after the technology readiness shifting is applied, the Solar collector strategy remains particularly competitive, despite the fact that the nuclear interceptor has better comparative performance in this table (only between 6 and 17% of the domain is still dominated by the solar collector method). It is also worth pointing out that the solar collector, along with all the other non-impulsive deviation techniques, does not present a risk of fragmentation and offers the possibility to accurately control the deviation action. For example, considering, as a first approximation, an energy density limit of 1 J/g^{25} , a nuclear interceptor with a yield of 5 Ktons or more would probably cause a fragmentation of an Apophis-size, or smaller, asteroid. This aspect definitively deserves a further investigation to better understand the consequences of a possible fragmentation for small to medium size asteroids.

VII. Conclusions

In this paper, a comparison of six different deflection strategies was presented: nuclear interceptor, solar collector, mass driver, low-thrust propulsion, gravity tug, and kinetic impactor. The comparison was based on four different criteria that translate quantitatively from a number of qualitative statements defining the performance of a particular deviation strategy: ease of deflection, cost of the mission, complexity of the approach, readiness of the deviation strategy, and response time.

The results from this study show that the solar collector and the nuclear interceptor options achieve the best results in terms of deviation, mass into space and warning time. The nuclear interceptor is better than the solar collector in the Apollo case and in the Apophis case after the application of the technology readiness shift in the warning time. On the other hand, the solar collector solutions dominate the nuclear interceptor in both the Apophis and Aten cases if no technology readiness shift is applied. Furthermore, it should be noted that despite the low technology readiness, the solar collector still remains competitive against most of the deflection methods.

Kinetic impactor and low-thrust display comparable performance, and both prove an interesting alternative for deviating asteroids with a mass below 10^{10} kg; particularly the kinetic impactor if the technology level is considered. Kinetic impactor performance is better for the Apollo class of asteroids, especially for short warning times, while low-thrust dominates in the Aten category, especially for long warning times.

The mass driver presents an intermediate performance between the the two pairs: solar collector – nuclear interceptor and kinetic impactor–low thrust, although its technology readiness is still considerably low compared to the kinetic impactor, and its performance is not as good as solar collector. It should be

noted that the estimation of the technology readiness of each deviation method is subject to the current and future political and economical situations. Therefore, a complete evaluation of the methods presented in this paper would require also considering the economical and political aspects in the development of a specific technology, which was not done in this analysis.

On the other hand, the comparison methodology proposed in this paper, based on the concept of set dominance, allowed us to compare two or more methods using sets of hundreds of solutions, each one representing a complete mission with a specific launch date and transfer time, instead of using a single typical or hypothetical mission case. Therefore, the comparison is not subject to any particular ideal or fictitious scenario in which the deflection method is applied, and takes into account the fact that for some methods some mission opportunities could be prohibitive or not feasible. Though in the paper we use only three quantitative criteria, the same procedure could be extended to a more extensive analysis including more figures of merit.

Finally, though the results in this paper cannot be used to rule out any of the analyzed deflection methods, they suggest some promising directions of research where the performance of a particular method is high but the technology readiness is still low.

VIII. Acknowledgements

The authors would like to thank Dr. Marco Guglielmi, Head of Technology Strategy Section of the European Space Agency, for the precious advice on the definition of the logistic function for the *TRL* mapping into development effort.

References

¹Stokes, G.H., and Yeomans, D.K., "Study to Determine the Feasibility of Extending the Search for Near-Earth Objects to Smaller Limiting Diameters," NASA Report of the Near-Earth Object Science Definition Team, Aug. 2003.

²"Near-Earth Objects Survey and Deflection Analysis of Alternatives," National Aeronautics and Space Administration, NASA Authorization Act of 2005, March 2007.

³Izzo, D., "On the deflection of Potentially Hazardous Objects," *15th AAS/AIAA Space Flight Mechanics Conference*, Copper Mountain, Colorado, AAS 05-141, Jan. 2005.

⁴Scheeres, D.J., and Schweickart, R.L., "The Mechanics of Moving Asteroids," *Planetary Defense Conference*, AIAA 2004-1446, AIAA, Orange County, California, Feb. 2004.

⁵Carusi, A., Valsecchi, G.B., D'abramo, G., and Bottini A., "Deflecting NEOs in Route of Collision with the Earth," *Icarus*, Vol. 159, No 2, 2002, pp. 417-422. doi:10.1006/icar.2002.6906

⁶Conway, B.A., "Near-Optimal Deflection of Earth-Approaching Asteroids," *Journal of Guidance, Control and Dynamics*, Vol. 24, No. 5, 2001, pp. 1035-1037.

⁷Park, S.Y, and Ross I.M., "Two-Body Optimization for Deflecting Earth-Crossing Asteroids," *Journal of Guidance, Control and Dynamics*, Vol. 22, No. 3, 1999, pp. 415-420.

⁸Ross, I.M., Park, S.Y., and Porter S.D.V., "Gravitational Effects of Earth in Optimizing Dv for Deflecting Earth-Crossing Asteroids," *Journal of Spacecraft and Rockets*, Vol. 38, No. 5, 2001, pp. 759-764.

⁹Hall, C.D., and Ross I.M., "Dynamics and Control Problems in the Deflection of Near-Earth Object," *Advances in the Astronautical Sciences*, Vol. 67, No. 640, 1997, pp. 1-18.

¹⁰MIT students. Project Icarus. 1968. The MIT Press.

¹¹Tedeschi, W.J., Remo, J.L., Schulze, J.F., and Young, R.P., "Experimental Hypervelocity Impact Effects on Simulated Planetary Materials," *International Journal of Impact Engineering*, Vol. 17, 1995, pp. 837-848.

¹²McInnes C., "Deflection of Near-Earth Asteroids by kinetics Energy Impacts from Retrograde Orbits," *Planetary and Space Science*, Vol. 52, No 7, 2004, pp. 587-590. doi:10.1016/j.pss.2003.12.010

¹³Smith, P.L., Barrera, M.J., Campbell, E.T., Fedman, K.A., Peterson, G.E., and Smit G.N., "Deflecting a Near Earth Object with Today's Space Technology," *Planetary Defense Conference*, AIAA 2004-1447, AIAA, Orange County, California, Feb. 2004.

¹⁴Lu, E.T., and Love, S.G., "Gravitational Tractor for Towing Asteroids," *Nature*, Vol. 438, Nov. 2005, pp. 177-178. doi:10.1038/438177a

¹⁵Spitale, J.N., "Asteroid Hazard Mitigation using the Yarkovsky Effect," *Science*, Vol. 296, No 5565, 2002, pp. 77. doi:10.1126/science.1069577

¹⁶Melosh, H.J., Nemchinov, I.V., and Zetzer, Y.I., "Non-nuclear Strategies for Deflecting Comets and Asteroids," *Hazard Due to Comets and Asteroids*, edited by T.Gehrels University of Arizona, 1994, pp. 1110-1131.

¹⁷Olds, J., Charania, A., and Schaffer, M.G., "Multiple Mass Drivers as an Option for Asteroid Deflection Missions," *Planetary Defense Conference*, AIAA 2007 S3-7, AIAA, Washington, D.C., March 2007.

¹⁸Schaub, H., and Junkins, J.L., *Analytical mechanics of space systems*, AIAA Education Series AIAA, Reston, 2003, pp. 592–623.

¹⁹Battin, R.H., *Introduction to the Mathematics and Methods of Astrodynamics*, AIAA Education Series, AIAA, Reston, VA, 1999, pp. 484-490.

²⁰Vasile M., and Colombo, C., "Optimal Impact Strategies for Asteroid Deflection". Accepted for publication, *Journal of Guidance, Control and Dynamics*, 2008. doi: 10.2514/1.33432

²¹Sagan, C., *Pale Blue Dot: A Vision of the Human Future in Space*, Random House, Toronto, 1994, pp.149-150.

²²Hammerling, P., and Remo, J.L., "NEO Interaction with Nuclear Radiation," *Acta Astronautica*, Vol. 36, No. 6, 1995, pp. 337-346.

²³S.Glasstone, *The Effects of Nuclear Weapons*, U.S. AEC 1962.

²⁴Wang, J., Davis, A.M., Clayton, R.N., and Hashimoto, A., "Evaporation of Single Crystal Forsterite: Evaporation Kinetics, Magnesium Isotope Fractionation, and Implications of Mass-dependent Isotopic Fractionation of a Diffusion-Controlled Reservoir," *Geochimica et Cosmochimica Acta*, Vol. 63, No. 6, 1999, pp. 953-966.

²⁵Holsapple K.A., "The Scaling of Impact Processes in Planetary Science". *Annual Review of Earth and Planetary Science*, Vol. 21, May 1993, pp. 333-373.

²⁶Scheeres, D.J., "Close Proximity Operations for Implementing Mitigation Strategies," *Planetary Defense Conference*, AIAA 2004-1445, AIAA, Orange County, California, Feb. 2004.

²⁷Wertz, J.R., and Larson, W.J., *Space Mission Analysis and Design*, Third ed., Microcosm Press 2003, pp. 703.

²⁸Olds, J., Charania, A., Graham, M., and Wallace, J., "The League of Extraordinary Machines: A rapid and Scalable Approach to Planetary defense Against Asteroid Impactors," Version 01, NASA Institute for Advanced Concepts (NIAC), CP-NIAC 02-02, Apr. 2004.

²⁹ Lehmann, P., Reck, B., Behrens, J., and Vo, M.D., "Acceleration of a Suborbital Payload Using an Electromagnetic Railgun," *IEEE Transactions on Magnetics*, Vol. 43, No. 1, 2007, pp. 480-485. doi:10.1109/TMAG.2006.887666

³⁰Ahrens, T.J., and Harris, A.W., "Deflection and Fragmentation of Near-Earth Asteroids," *Nature*, Vol. 360, Dec. 1992, pp. 429-433. doi:10.1038/360429a0

³¹Anttila, M. and Ylikorpi, T., "Defining the Technical Requirements for Subsurface Mars Driller," *Sixth International Conference on Mars*, paper 3020, Pasadena, California. July 2003.

³²Liu, Y., Weinberg, B., and Mavroidis, C., "Mechanical Design and Modelling of a Robotic Planetary Drilling System," *ASME 2006 International Design Engineering Technical Conferences & Computers and Information in Engineering Conference*, DETC2006-99699, Philadelphia, Pennsylvania, USA. Sep. 2006.

³³Thomas, M., "Inflatable Space Structures," *IEEE Potentials Magazine*, Vol. 11, No. 4, 1992, pp. 29-32. doi:10.1109/45.207143

³⁴Hedgepeth J.M., and Miller R.K., "Structural concepts for large solar concentrators," *Acta Astronautica*, Vol. 17, No. 1, 1988, pp. 79-89. doi:10.1016/0094-5765(88)90131-2

³⁵Harris, A.W., "The Rotation Rates of Very Small Asteroids: Evidence for 'Rubble Pile' Structure," *Lunar and Planetary Science*, Vol. 27, 1996, pp. 493.

³⁶Maddock, C., Sanchez, J.P., Vasile, M., and Radice, G., "Comparison of Single and Multi-Spacecraft Configurations for NEA Deflection by Solar Sublimation," *New Trends in Astrodynamics and Applications*, Princeton, New Jersey, AIP Conference proceedings, Vol. 886, 2007, pp. 303-316.

³⁷Vasile, M., "A Multimirror Solution for the Deflection of Dangerous NEOs," *2nd Conference on Nonlinear Science and Complexity*, Porto, Portugal, July 2008.

³⁸McInnes, C., "Near Earth Object Orbit Modification Using Gravitational Coupling," *Journal of Guidance, Control and Dynamics*, Vol. 30, No. 3, 2007, pp. 870-873.

³⁹Broschart, S.B., and Scheeres, D.J., "Control of Hovering Spacecraft Near Small Bodies: Application to Asteroid 25143 Itokawa," *Journal of Guidance, Control and Dynamics*, Vol. 28, No. 2, 2005, pp. 343-354.

⁴⁰Kawaguchi, J., Fujiwara, A., and Uesugi, T., "Hayabusa—Its technology and science accomplishment summary and Hayabusa-2," *Acta Astronautica*, Vol. 62, No. 10-11, 2008, pp. 639-647. doi:10.1016/j.actaastro.2008.01.028

⁴¹Vasile, M., "Robust Mission Design Through Evidence Theory and Multiagent Collaborative Search," *Annals of the New York Academy of Sciences*, Vol. 1065, Jan. 2006, pp. 152-173.

⁴²Vasile, M., "A Hybrid Multi-Agent Collaborative Search Applied to the Solution of Space Mission Design Problems," *Global Optimization Workshop*, Almeria, Spain, Sep.2005.

⁴³Valsecchi, G. B., "Close encounters and collisions of Near-Earth asteroids with the Earth," *Comptes Rendus Physique*, Vol. 6, No. 3, 2005, pp. 337-344. doi:10.1016/j.crhy.2004.12.014

⁴⁴De Pascale, P., and Vasile, M., "Preliminary Design of Low-Thrust Multiple Gravity Assist Trajectories," *Journal of Spacecraft and Rockets*, Vol. 43, No. 5, 2006, pp. 1065-1076.

⁴⁵Mankins, J.C., "Approaches to Strategic Research and Technology (R&T) Analysis and Road Mapping," *Acta Astronautica*, Vol. 51, No. 1-9, 2002, pp. 3-21. doi:10.1016/S0094-5765(02)00083-8

⁴⁶Moorhouse, D.J., "Detailed Definitions and Guidance for Application of Technology Readiness Levels," *Journal of Aircraft*, Vol. 39, No. 1, 2001, pp. 190-192.

⁴⁷Ferri, P., and Schwehm, G., "Rosetta: ESA's Comet Chaser Already Making its Mark," *ESA bulletin*, Vol. 123, pp. 62-66, Aug. 2005.

⁴⁸Blacic, J., Dreesen, D., and Mockler, T., "Report on Conceptual System Analysis of Drilling Systems for 200-m-Depth Penetration and Sampling of the Martian Subsurface", Technical Report LAUR00-4742, Los Alamos National Laboratory, Oct. 2000.

⁴⁹Basso, B, Bartlett, P., Gorevan, S., Kennedy, T., Paulsen, G., Wilson, J., and Yachbes, I., "Surface Anchoring and Deflection Concepts for Earth-crossing Comets and Asteroids," *Workshop on Spacecraft Reconnaissance of Asteroid and Comet Interiors*, paper 3032, Santa Cruz, California, Oct. 2006.

⁵⁰Vorontsov, M.A., Kolosov, V.V, and Kohnle, A, "Adaptive Laser Beam Projection on an Extended Target: Phase- and Field-conjugate Precompensation," *Journal of the Optical Society of America*, Vol. 24, No. 7, 2007, pp. 1975-1993.

⁵¹Angel, R., Burge, J., Hege, K., Kenworthy, M., and Woolf, N., "Stretched Membrane with Electrostatic Curvature (SMEC): A New Technology for Ultra-lightweight Space Telescopes," *UV, optical, and IR space telescopes and instruments*, Vol. 4013, 2000, pp. 699-705.

⁵²Composite ultra-light weight active mirror for space applications. [7064885]. 4-10-2005. Patent of United States.

⁵³"A New Deployable Thin-film, Ultralight Mirror for Future Space Telescopes and Surveillance Satellites," *Current Science*, Vol. 79, No. 1, 2000, pp. 12.

